10 EUR

HUNGARIAN GROUP OF *fib*

# CONCRETE STRUCTURES

ANNUAL TECHNICAL JOURNAL



2021

Vol. 22

**CONCRETE STRUCTURES**
Journal of the Hungarian Group of ***fib***



Founded by: Hungarian Group of ***fib***
Publisher: Hungarian Group of ***fib***
(***fib*** = International Federation for Structural Concrete)

**Editorial office:**
Budapest University of Technology and Economics (BME)
Department of Construction Materials and Engineering Geology
Műegyetem rkp. 3., H-1111 Budapest
Phone: +36-1-463 4068
Fax: +36-1-463 3450
WEB http://www.fib.bme.hu
WEB editor: András Bíró

Layout and print: Csaba Halmai, Navigar Ltd.

Price: 10 EUR, Printed in 1000 copies


HU ISSN 2062-7904
online ISSN: 1586-0361

Cover photo: Multi level reinforced concrete water tower, La Digue, Seychelles

Photo by György L. Balázs

# CONTENT



Sponsors:

Railway Bridges Foundation, ÉMI Nonprofit Ltd., HÍDÉPÍTÕ Co., Holcim Hungary Co., MÁV Co., MSC Consulting Co., Lábatlani Vasbetonipari Co., Pont-*TERV* Co., UVATERV Co., MÉLYÉPTERV KOMPLEX Engineering Co., SW Umwelttechnik Hungary Ltd., Betonmix Consulting Ltd., BVM Épelem Ltd., CAEC Ltd., Pannon Freyssinet Ltd., STABIL PLAN Ltd., UNION PLAN Ltd., DCB Consulting Ltd., BME Dept. of Structural Engineering, BME Dept. of Construction Materials and Technologies

# THE TENSILE STRENGTH: THE MOST FUNDAMENTAL MECHANICAL CHARACTERISTICS OF CONCRETE

Andor Windisch

https://doi.org/10.32970/CS.2021.1.1

*Concrete is an inhomogeneous building material. It has a considerable and reliable compressive strength and a relative low tensile strength which can be even exhausted locally under unfortunate conditions. It is quite obvious that the concrete tensile strength was always reprehended as the most unreliable concrete property.*

*A simple relationship between tensile- and compressive strength is introduced. The mechanical background of the relation tensile- to compressive strength in case of 'normal' and high strength concretes is elucidated. Mechanical bond, too, relies completely on the tensile strength. In the design of structural concrete members the tension fields are more characteristic than the compression fields. Effective concrete strengths are not successful. Tensile strength can be applied as 'yield condition' for the lower bound solution in the theory of plasticity.*

*The paper intends to contribute to the acceptance of the tensile strength as the more fundamental concrete characteristics.*

**Keywords:** tensile strength, compressive strength, bond, lower bound theorem

## 1. INTRODUCTION

Concrete is an inhomogeneous building material. It has a considerable and reliable compressive strength and a relative low tensile strength which can be even exhausted locally under unfortunate conditions, e.g. due to hydration heat of cement or to its plastic shrinkage. It is quite obvious that the concrete tensile strength was always reprehended as the most unreliable concrete property.

As the compressive strength of the conventional test specimens (cubes or cylinders) was rather insensitive to most of the aforementioned influences and it was convenient to be measured, it became accepted by the material science, the design office and the construction site as the fundamental mechanical characteristics of concrete.

Several other properties were deduced empirically by the help of best-fit formulas using the compressive strength as basic variable.

According to a sad terminology, students learn to 'neglect' the concrete tensile strength at dimensioning any SC member. Even Model Codes use this verb. In other standards and notebooks tensile strength will be 'ignored'. At dimensioning of watertight or prestressed concrete structures the tensile strength will be relied on with a shy consciousness of guilt.

Reinforced concrete consists of: concrete, reinforcement, discrete cracks and bond.

Loaded in axial tension concrete fails to longitudinal elongation, loaded in axial compression it fails to transversal elongation. In practice these failures are characterized with the stresses deduced from the failure load divided with the specimen's nominal cross section area perpendicular to the direction of the failure load. A special tension loading/failure type is the inclined splitting of concrete cover due to dowel action of a rebar. Here neither the acting load level nor the effected concrete surface is known thus practical detailing rules are given in order to eliminate this type of concrete failure.

Tensile strength is the most fundamental characteristics of concrete.

This paper intends to contribute to the acceptance of the tensile strength as the more fundamental concrete characteristics.

## 2. THE 'ROLE' OF TENSILE STRENGTH AT THE COMPRESSIVE STRENGTH

Concrete has three constituents: the aggregate, the cement matrix and the bond on the interface between them. Both, the aggregates and the matrix have their Young's Modulus and Poisson's ratio and a bond strength. In concrete classes, say, C50, $E_{ag} > E_{cem}$, Loading a specimen in uniaxial compression (deformation) the compressive trajectories 'run' from the aggregate to aggregate like in a motocross-course. The change of direction of the compressive trajectories cause tensile stresses between the aggregate and cement matrix. The specimen fails at a relative low compressive strength, the ratio compressive to tensile strength is relative low, nevertheless the practice since the beginning of reinforced concrete

construction accustomed to praise the low/normal strength concretes on account of its relative high tensile strength.

At design of high strength concretes the concrete technologist knowingly or out of habit improves the Young's Modulus of the cement matrix. Loading a specimen in uniaxial compression (deformation) the compressive trajectories 'run' straight through aggregate and matrices, the bond strength between aggregate and matrix is barely loaded: the specimen fails at a relative high compressive strength. The practice reprehends the high strength concretes for their relative low tensile strength, although HC and UHC should be praised for their relative high compressive strength. Of course in case of loading which causes direct tensile stresses the 'lower' tensile strength should be taken into account.

At design of high strength lightweight concretes the concrete technologist (knowingly or out of habit) reduces the Young's Modulus of the cement matrix to the relative low $E_{ag}$ of the lightweight aggregate, thus achieving a relative homogenous material, due to the 'straight' compressive trajectories a relative high compressive strength will be achieved.

Do we neglect the concrete tensile strength at calculation of ultimate flexural moment?

We do not neglect it at all: the flexural failure occurs in a cracked section where the tensile strength has been exceeded.

Note: The conical failure patterns (well-known from the usual compression tests) are the 'results' of the influence of the friction between the steel loading plate and the specimen, hence causes a false perception in the superficial viewer. Concrete is not a frictional material at all. The Mohr-Coulomb material law is not valid in case of concrete.

## 3. RATIO OF COMPRESSIVE TO TENSILE STRENGTH

In MC2010 the mean value of uniaxial tensile strength $f_{ctm}$ in [MPa] is defined as:

$f_{ctm} = 0.3\,(f_{ck})^{2/3}$ for concrete grades ≤ C50

$f_{ctm} = 2.12\,\ln(1 + 0.1(f_{ck} + 8))$ for concrete grades > C50

.

Defining the ratio

$$\chi = f_{ck}/f_{ctm} \quad (1)$$

we get it as function of the characteristic compressive strength, $f_{ck}$ (*Figure 1*).

*Figure 1* reveals that the simple linear function

$$\chi = 0.13\,f_{ck} + 6 \quad (2)$$

describes quite exactly the interrelation of tensile to compressive strengths, hence $f_{ctm} = f_{ck} / \chi$ .

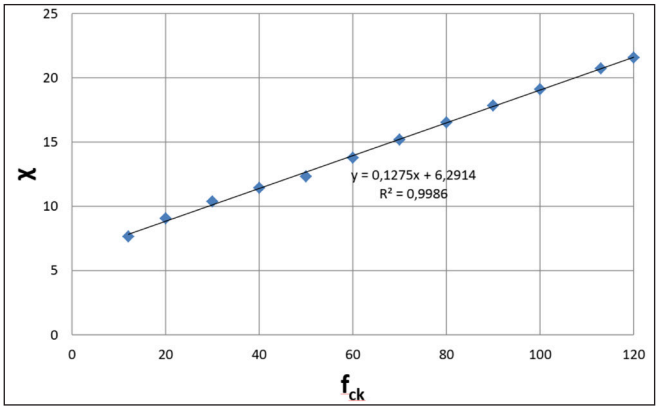


**Figure 1:** Ratio of compression strength to tensile strength (χ) as function of $f_{ck}$

this showing different powers < 1 of the mean concrete compressive strength. (Such terms always stay in formulas and equations substituting the tensile strength, which is neglected by the modern r.c. theories and models, isn't it?

*Figure 2* shows the analytical bond stress-slip relationship as given in MC 2010.

The mechanical bond between rebar and the concrete around develops when relative displacement occurs between them. The rebar's ribs are supported by the concrete brackets, as shown in *Figure 3*. The slip, as shown in *Figure 2* comes from the deformation of the concrete brackets. The compressive stresses loading the brackets let develop longitudinal and circular tensile stresses, and then first internal cracks (in red in *Figure 3*) which are called Goto-cracks (after the researcher who first showed them). The curved course of the bond stress-slip relationship reveals the influence of

**Figure 2:** Analytical bond stress-slip relationship (monotonic loading) acc. to MC 2010 (2013)

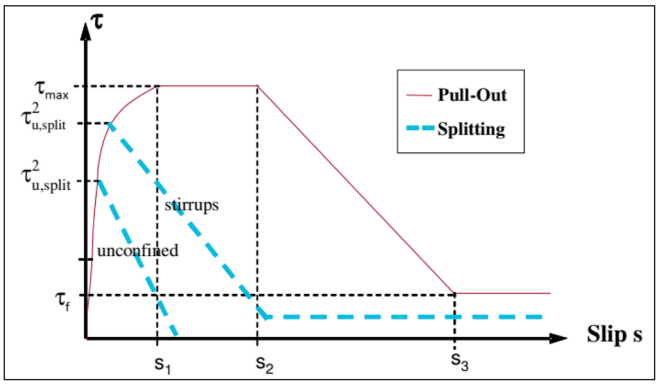


**Table 1:** Parameters defining the mean bond stress-slip relationship of deformed bars acc. to MC 2010 (2013)

| | 1 | 2 | 3 | 4 | 5 | 6 |
|---|---|---|---|---|---|---|
| | Pull-Out (PO) | | Splitting (SP) | | | |
| | $\varepsilon_s < \varepsilon_{s,y}$ | | $\varepsilon_s < \varepsilon_{s,y}$ | | | |
| | Good bond cond. | All other bond cond. | Good bond cond. | | All other bond cond. | |
| | | | unconfined | stirrups | unconfined | stirrups |
| $\tau_{max}$ | $2.5\sqrt{f_{cm}}$ | $1.25\sqrt{f_{cm}}$ | $7.0\cdot\left(\frac{f_{cm}}{25}\right)^{0.25}$ | $8.0\cdot\left(\frac{f_{cm}}{25}\right)^{0.25}$ | $5.0\cdot\left(\frac{f_{cm}}{25}\right)^{0.25}$ | $5.5\cdot\left(\frac{f_{cm}}{25}\right)^{0.25}$ |
| $s_1$ | 1.0mm | 1.8mm | $s(\tau_{max})$ | $s(\tau_{max})$ | $s(\tau_{max})$ | $s(\tau_{max})$ |
| $s_2$ | 2.0mm | 3.6mm | $s_1$ | $s_1$ | $s_1$ | $s_1$ |
| $s_3$ | $c_{clear}$ [1)] | $c_{clear}$ [1)] | $1.2s_1$ | $0.5c_{clear}$ [1)] | $1.2s_1$ | $0.5c_{clear}$ [1)] |
| $\alpha$ | 0.4 | 0.4 | 0.4 | 0.4 | 0.4 | 0.4 |
| $\tau_f$ | $0.40\,\tau_{max}$ | $0.40\,\tau_{max}$ | 0 | $0.4\,\tau_{max}$ | 0 | $0.4\,\tau_{max}$ |

1) $c_{clear}$ is the clear distance between ribs

## 4. BOND

Without mechanical bond the higher strength rebars could not be exploited economically, the triumphal march of reinforced concrete in the last over 70 years would not be possible.

Bond is a direct consequence of concrete tensile strength, even if *Table 1* taken form MC 2010 (2013) deftly conceals

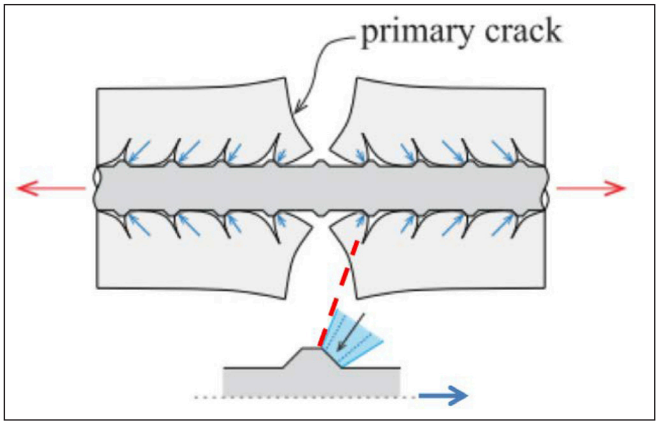


**Figure 3:** Primary- and Goto-cracks, compressive stresses and crack development at a rebar´s rib

the Goto-cracks: the stiffness of bond decreases. In extensive pull-out tests in the Laboratory of the Institute for Reinforced Concrete Structures of TU Budapest, Hungary, Windisch (1984, with the active support of Balázs, that time student there) showed that the bond parameters - identical to $s_3$ - $s_1$ and $s_2$, too depend on the clear rib spacing, hence on the bar diameter. Therefore the constant values given in MC 2010 are not correct. Moreover, in the more than 300 PoT-s the slips on both, loaded and unloaded ends of the specimens were measured: the slips on the unloaded ends show a much stiffer bond characteristics than those measured on the loaded one (Windisch, 1985). Nevertheless, MCs and the producers of FEM models do not take this into account. What a pity!

Increasing the slip the circular tensile stresses around the rebars increase as well. These can cause the longitudinal splitting of the concrete cover which further decreases the bond-stiffness or even leads to total loss if bond (blue lines in *Figure 2*).

Bond completely relies on the tensile strength of concrete.

## 5. MODELS FOR REINFORCED CONCRETE MEMBERS: COMPRESSION FIELD OR TENSION FIELD?

Soil has, similar to concrete a low tensile strength compared to its compressive strength. Experts of soil mechanics continued to check form, position and load bearing capacity of sliding surfaces in soil structures even after introduction of the theory of plasticity.

Similar to soil structures, the condition of structural concrete members can/could be better described with tension fields than with compression fields, unless the member will become over-reinforced.

Models operating with compression fields (Strut-and-Tie, Modified Compression Field Theory and others) adjust their predicted capacities to the test results applying efficient compressive strength values. Nevertheless, during the decades and hundreds of different applications no generally valid efficient compressive strength value has been found. Each test yield different efficiency factors. The fundamental problem is that in most of the cases compression is not the fundamental variable. A characteristic example is a dapped end with usual reinforcing pattern tested by Desnerck et al. (2018): NS-REF made of C30/37 failed at 402 kN whereas LS-REF (C12/15) at 400 kN. Try to define here a common efficiency factor! For this reason STM and MCFT have - no matter how well they are marketed – no future.

## 6. APPLICATION OF TENSILE STRENGTH IN THE THEORY OF PLASTICITY

In the theory of plasticity for the approximation of the failure load two limit values can be determined: according to the lower limit - and the upper limit theorem, resp.

Lower bound theorem:

The structure won't collapse if only it is possible to find a statically admissible stress field corresponding with the load. In such situation the bearing capacity is at least the same as the corresponding load or even higher.

Statical admissibility of the stress field requires that:

- stress field is in equilibrium with external load,
- stress field satisfies the internal equilibrium condition,
- stress field satisfies the statical boundary conditions,
- stress do not exceed the limit value.
- a proportional increase in load is assumed. i.e. all loads remain proportional to each other. This allows the entire load system to be controlled with one load parameter. If this is not the case, the load combinations must be examined individually.

If an equilibrium distribution of stress can be found which balances the applied load and nowhere violates the yield criterion, the body (or bodies) will not fail, or will be just at the point of failure.

Upper bound theorem:

The structure will collapse, if only it is possible to find a kinematically admissible velocity field such that total work of external load is not less than total work of internal forces. The bearing capacity is at most the same as the one correspondingly with the load, but it may be lower.

Kinematic admissibility of the velocity field requires that

- velocity field satisfies the kinematic boundary conditions
- velocity field is such that displacement is continuous
- total work of external load on velocity is positive.
- a state of motion is kinematically permissible if the resistance and motion correspond to the flow condition and the flow law and the geometric boundary conditions are observed.
- A mechanism is a kinematically permissible state of motion and has one degree of freedom.

Applying the lower bound theorem in case of concrete structures then the tensile strength can be considered as yield criterion, too.

The notion: "yield condition" and the very often pronounced reference: "tensile strength of concrete will be neglected" led to erroneous perceptions concerning the tensile strength of concrete:

Lower bound failure loads in case of (the letters in italic mark the relevant 'yield criterion'):

- plain concrete members loaded in uniaxial tension

$$N_u = A_c * f_{ct}$$

- unreinforced concrete members loaded in pure flexure

$$M_u = W_c * f_{ct}$$

Conclusion: the well-known cracking loads are lower bound values.

## 7. CONCLUSIONS

The tensile strength of concrete is the most fundamental mechanical characteristics of concrete. The compressive strength is a cleverly used tensile strength. The test specimens loaded in pure compression fail when discrete tensile cracks perpendicular to the direction of the compressive load occur. This is valid in case of 2D and 3D compressive loading, too.

Mechanical bond is based on the concrete tensile strength around the rebars. Codes should give direct reference to the role of tensile strength at bond problems.

As in many cases the ultimate load of reinforced concrete members are quite insensitive to variation of the compressive strength, hence models where the basic variable is the effective compressive strength face with serious problems.

The tensile strength of concrete is a fully valid yield criterion for determination of failure loads according to the lower limit theorem.

## 8. REFERENCES


Desnerck, P., Lees, J. M., and Morley, C. T., (2018), "Strut-and-tie models for deteriorated reinforced concrete half-joints", *Engineering Structures* 161 Elsevir Ltd. pp. 41-54.

MC2010, (2013) "*fib* Model Code for Concrete Structures 2010" *Ernst und Sohn, Wiley*, ISBN 978-3-433-03061-5

Windisch A., Balázs L.Gy., (1984), "A beton és az acélbetét együttdolgozását jellemzö α-értékekröl" (On the α-values characterizing the bond between concrete and rebars.) *Mélyépítéstudományi Szemle*, Vol. XXXIV, pp. 262-264.

Windisch A., Balázs L.Gy., (1984), "A beton és az acélbetét együttdolgozásának jellemzése a fajlagos kapcsolati erő – relativ elmozdulás összefüggéssel" (Characterization of the bond between concrete and rebars with the relative bond force - relative displacement function.), *Mélyépítéstudományi Szemle*, Vol. XXXIV, pp. 265-271.

Windisch, A., (1985), "A modified Pull-Out-Test and new evaluation methods for a more real local bond-slip relationship", Matériaux et Constructions, No. 105, https://doi.org/10.1007/BF02472967

Windisch, A. (1991), "Tensile strength concrete: prodigal son or primary source?", *IABSE Colloquium Stuttgart*, ETH-Hönggerberg, Zürich, Switzerland, pp. 773-777.


## NOTATIONS

| | |
|---|---|
| $A_c$ | ideal concrete area |
| $E_{ag}$, $E_{cem}$ | Young's Modulus of elasticity of aggregates and cement matrix, resp. |
| $N_u$, $M_u$ | Ultimate cracking tensile force and bending moment of plain concrete members |
| $W_c$ | Cross section modulus of uncracked concrete cross section |
| $c_{clear}$ | clear distance between ribs |
| $f_{ck}$ | characteristic value of concrete compressive strength, MPa |
| $f_{ctm}$ | mean value of uniaxial concrete tensile strength, MPa |
| $s_1$, $s_2$, $s_3$ | characteristic slip values of the analytical bond stress-slip relationships |
| $\chi$ | ratio of characteristic value of concrete compressive strength to uniaxial concrete tensile strength |
| $\tau$ | bond stress values |


**Andor Windisch PhD, Prof. h.c.** retired as Technical Director of Dywidag-Systems International in Munich, Germany. He made his MSc and PhD at Technical University of Budapest, Hungary, where he served 18 years and is now Honorary Professor. Since 1970 he is member of different commissions of FIP, CEB and ***fib***. He is author of more than 180 technical papers. Andor. Windisch@web.de

# COMPARISON OF THE RESULTS OF NOTCHED THREE POINT BENDING TEST WITH MODEL CODE 2010 FORMULAS

Viktor Hlavicka

https://doi.org/10.32970/CS.2021.1.2

*The primary application of the notched three point bending test (3PBT) is to determine the fracture energy of concrete. However, the measurement setup is also suitable for determining additional mechanical parameters: flexural tensile strength, modulus of elasticity, and indirectly the compressive strength also. The aim of this paper is to present the calculation methods of the mechanical properties that can be determined from the results of a test series in which mixtures with different types of aggregates were used (quartz, dolomite, limestone, andesite, expanded clay). To validate the obtained results, the parameters determined from the measurements are compared to the formulas of the fib Model Code 2010. A recommendation is also presented for the calculation of the fracture energy by using compressive strength values measured on a half prism.*

**Keywords:** thermally damaged concrete, three point bending test (3PBT), crack mouth opening displacement (CMOD), fracture energy

## 1. INTRODUCTION

Depending on the shape and the behaviour of the fracture process zone around a crack tip, construction materials can be classified as brittle, quasi-brittle and elastic-plastic. Concrete belongs to the quasi-brittle category (*Khalilpour, BaniAsad, and Dehestani*, *2019*; *Rao and Rao*, *2014*). Concrete, as a construction material, contains micro-cracks, pores, potential failure locations even without loads (*Sólyom, Di Benedetti, and Balázs*, *2021*). During loading the number of cracks and failure locations increase and affect the behaviour and load-bearing capacity of the material (*Fehérvári, Gálos, and Nehme*, *2010a*). As a result of the internal forces, the micro-cracks start to form larger cracks and above a critical level crack opening and propagation accelerate (*Bažant and Planas*, *1997*). Understanding the behaviour of cracks is essential for the applicability of structural materials, as failure processes begin at potential failure locations (*Griffits*, *1921*). Fracture mechanics deals with the analysis of stress conditions around cracks and with the determination of the parameters affecting the opening and propagation of the cracks. In fracture mechanics the toughness of materials is most frequently characterised by two parameters: fracture energy ($G_f$) and critical stress intensity factor (K). Fracture energy is the energy required for the opening and propagation of the unit area of a crack (*Hillerborg, Modéer, and Petersson*, *1976*; *Khalilpour et al.*, *2019*), while the critical stress intensity factor characterises the resistance against rapid, uncontrolled crack propagation, introduced by *Irwin* (*Irwin*, *1957*), who also classified cracks by the main failure mode causing them: mode I is opening (tension), mode II is sliding (in plane shear), mode III is tearing (out of plane shear).

In case of concrete and reinforced concrete structures, typically tensile cracks (mode I) are analysed. The most common experimental method to investigate this failure is the notched 3PBT (*Khalilpour et al.*, *2019*). Prior to the test a crack-starting notch is made in the concrete specimen (it can be formed by sawing before testing or already during concreting), the height of the notch depends on the applied standards and recommendations, typically 1/6 - 1/2 of the specimen's height is used (*EN 14651:2005+A1*, *2007*; *Hillerborg*, *1985*; *JCI-S-001-2003*, *2003*; *RILEM Technical Committee 50 FMC*, *1985*). There are different versions of the experimental setup of 3PBTs. If the supports are located close to the edges of the specimen, then after the opening of a certain critical crack (*Fig. 1a*), the specimen cracks due to gravity, independently of all other loads. In this case the total fracture energy cannot be measured, but it can be corrected during the evaluation of the results (*JCI-S-001-2003*, *2003*; *RILEM Technical Committee 50 FMC*, *1985*). In order to balance the effect of self-weight, the measurement setup can also be designed so that the specimen extends significantly beyond the supports (*Fig. 1b*) or additional weights are placed at the ends of the beam (*Fig. 1c and 1d*) (*Kaplan*, *1961*). The adequate size of the specimen highly depends on the maximum aggregate size ($d_{max}$). Typically, even the smallest dimension of the specimen should be larger than 4 times $d_{max}$ (*JCI-S-001-2003*, *2003*); otherwise, the aggregate size will affect the value of the fracture energy.

The primary application of the notched 3PBT is to determine the fracture energy of concrete. However, the measurement setup is also suitable for determining additional mechanical parameters: flexural tensile strength, modulus of elasticity, and indirectly also the compressive strength. The aim of this paper is to present the calculation methods of the mechanical properties that can be determined from the test results of 3PBTs.

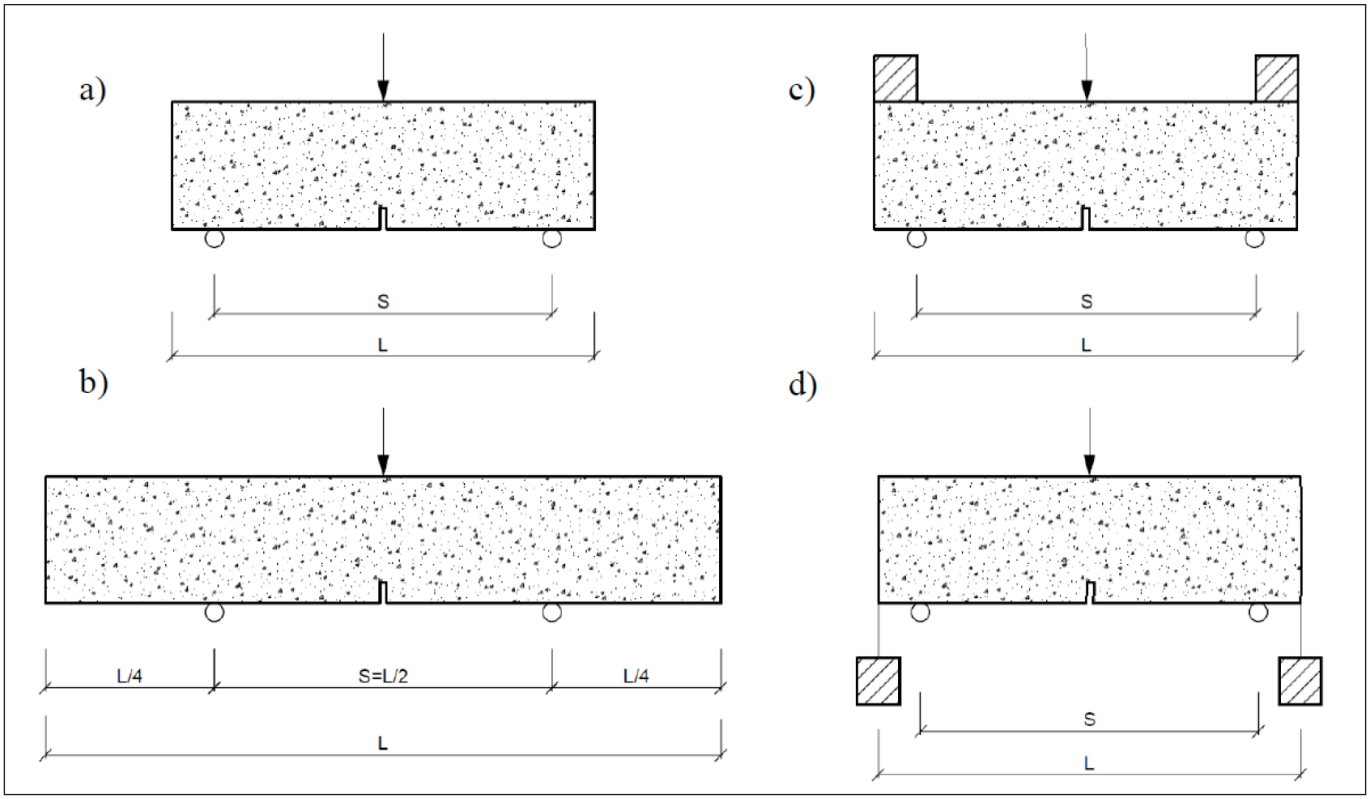


**Fig. 1:** Notched 3PBTs: a) general; take into account the gravity b) with overhang, c) and d) with weights

# 2. EXPERIMENTAL DETAILS

## 2.1 Materials

During our tests, 7 types of aggregates were used. In normal concretes (NCs), the most typical river quartz gravel, sand and mined dolomite, limestone and andesite were used, while in lightweight concretes (LWCs), two types of expanded clay aggregates (ECAs) were applied.

The shape of quartz aggregate and ECA was rounded: in case of quartz due to river fragmentation, while in case of ECA due to the technological process. The shape of the dolomite, limestone and andesite aggregate was angular due to the crushing process.

In case of the limestone aggregate, the body density was 2710 kg/m$^3$, which was available from the data given by the mine. For the other aggregates, the body density was determined by own measurements. The body density of the quartz gravel aggregate was 2645 kg/m$^3$, that of the dolomite aggregate was 2850 kg/m$^3$, and that of the andesite aggregate was 2700 kg/m$^3$. The body density of ECAs was 1465 kg/m$^3$ in case of type D1 and 1048 kg/m$^3$ in case of type D2. In case of lightweight aggregates, their high porosity causes high water absorption, which also affects the water-cement ratio of the concrete mixture *(Nemes and Józsa, 2006)*; therefore, the ECAs were saturated with water. After 30 minutes of water absorption, the body density of type D1 was 1549 kg/m$^3$, while that of type D2 was 1262 kg/m$^3$. The amount of absorbed water was taken into account during the correction of the concrete mixtures.

The type of cement applied in our mixtures was CEM III/32.5 R containing slag. The water-cement ratio was 0.45. The consistency of fresh concretes was F4 (*EN 12350-5:2019*, *2019*) which was regulated by the addition of superplasticiser (BASF Glenium C300). The fraction 0/4 mm was quartz sand in all the mixtures when fraction 4/8 mm was used. In order to make the comparison of the mixtures with different aggregates possible, it was important to evolve a similar aggregate skeleton; therefore, similar cement content, aggregate content and size distribution (0/4 mm 43%; 4/8 mm 57%) were applied. The concrete composition of different mixtures is summarised in *Table 1.*

The casted specimens were stored under water for 7 days and then in a climate chamber (temperature: 20 °C, relative humidity: 50 %). Tests of specimens were performed at 60 days of age.

## 2.2 Test equipment

In order to determine the fracture energy, crack mouth opening displacement (CMOD) controlled 3PBTs were carried out. The test setup is shown in *Fig.* 2. The applied CMOD controlled method is different from the previously recommended crosshead displacement controlled method (*Hillerborg*, *1985*; *RILEM Technical Committee 50 FMC*, *1985*), but it is accepted by many standards (*EN 14651:2005+A1*, *2007*; *JCI-S-001-2003*, *2003*). The force-CMOD curves derived by the two methods are the same (*Lee and Lopez*, *2014*). The size of the applied specimens was 70x70x250 mm. Based on literature this size is big enough to make the effect of aggregate size negligeable in case of 8 mm maximum aggregate size (*Fehérvári, Gálos, and Nehme*, *2010b*; *Hillerborg*, *1985*; *JCI-S-001-2003*, *2003*; *RILEM Technical Committee 50 FMC*, *1985*). The distance between the supports was 200 mm. The width of the notch was 4 mm, and its height was one sixth (12.5 mm) of the total height of the specimen. Crosshead displacement, CMOD and force were detected during the tests. During loading, the rate of CMOD was kept constant (0.01 mm/s).

The compressive strength of the concrete mixtures was determined by two methods. The compressive strength of cubes with the size of 150x150x150 mm was measured

**Table 1:** Concrete mix designs for 1 m³ (quantities are in kg)

| Unit weight | | Mixture symbol | | | | | | | |
|---|---|---|---|---|---|---|---|---|---|
| | | 4S | 4S8Q | 4D | 4S8D | 4S8L | 4S8A | 4S8D1 | 4S8D2 |
| Aggregate | sand (0/4 mm) | 1391 | 782 | - | 782 | 782 | 782 | 782 | 782 |
| | quartz (4/8 mm) | - | 1037 | - | - | - | - | - | - |
| | dolomite (0/4 mm) | - | - | 1499 | - | - | - | - | - |
| | dolomite (4/8 mm) | - | - | - | 1118 | - | - | - | - |
| | limestone (4/8 mm) | - | - | - | - | 1063 | - | - | - |
| | andesite (4/8 mm) | - | - | - | - | - | 1059 | - | - |
| | expanded clay D1 (4/8 mm) | - | - | - | - | - | - | 574* | - |
| | expanded clay D2 (4/8 mm) | - | - | - | - | - | - | - | 411* |
| Cement (CEM III/32.5 R): | | 600 | 390 | 600 | 390 | 390 | 390 | 390 | 390 |
| Water: | | 270 | 175 | 270 | 175 | 175 | 175 | 175 | 175 |
| w/c ratio | | 0.45 | 0.45 | 0.45 | 0.45 | 0.45 | 0.45 | 0.45 | 0.45 |
| Superplasticizer: | | 0.3 | 0.78 | 0.45 | 1.79 | 2.4 | 3.5 | 0.4 | 0.2 |

** calculated with dry body density of aggregate*

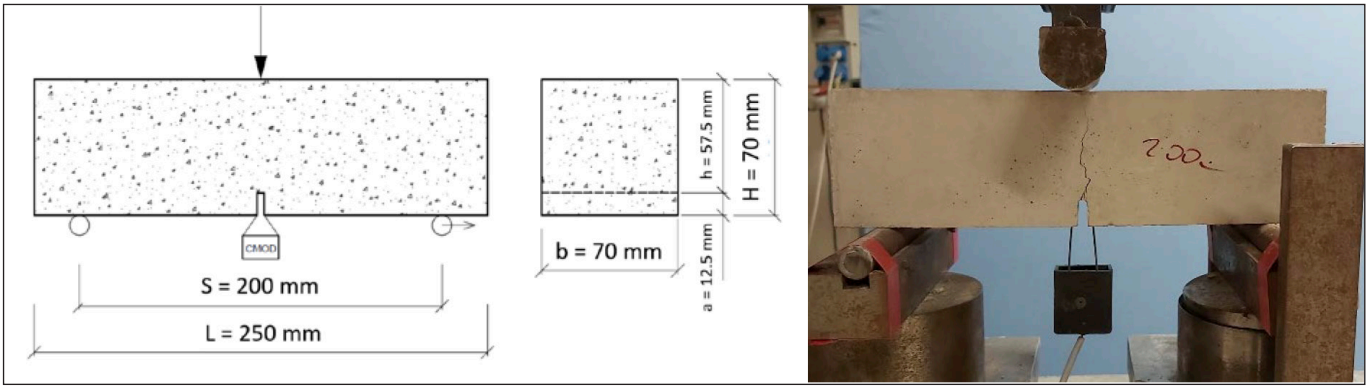


**Fig. 2:** Setup of the 3PBT

according to the standard *EN 12390-3* (*EN 12390-3:2019*, *2019*). Compressive strength was also measured on half prisms previously subjected to 3PBT (*Fig.* 3) (*Alimrani and Balazs*, *2020*; *Lublóy, Balázs, and Czoboly*, *2013*), where the load was transferred by steel plates with the size of 70x70 mm, which was the same as the width of the prism.

Mechanical tests were extended by measurements of moisture content and apparent porosity, which were measured on one half of the prisms. To determine moisture content, half prisms were dried in a drying furnace at 60 °C until constant mass. Initial moisture content could be calculated by the difference between the original and the dried mass. After drying, the specimens were stored under water until constant mass, therefore the amount of water uptake could be measured, and the volume of open pores could be determined (*EN 1936:2007*, *2007*).

**Fig. 3:** Compressive strength test: a) cube; b) half prism

# 3. RESULTS AND DISCUSSION

## 3.1 Body density, moisture content and apparent porosity

Dry body density values (*Table 2*) of the mixtures with ECA (4S8D1, 4S8D2) were lower than 2000 kg/m$^3$, therefore they could be considered as LWC (*fib BULLETIN 8*, *2000*; *fib MC2010*, *2013*). As expected, the apparent porosity of LWC mixtures was high due to the high porosity of aggregate particles. The apparent porosity of the mixture containing quartz sand only (4S) and dolomite sand only (4D) was also high. The mixtures with dolomite gravel (4S8D) and andesite gravel (4S8A) had the highest body density and consequently the lowest apparent porosity and moisture content.

## 3.2 Compressive strength

The *fib* Model Code 2010 (*fib MC2010*, *2013*) calculates the mechanical parameters by using the compressive strength of concrete. Therefore, in addition to 3PBTs, compressive strength tests were also performed using cubes and half prisms previously subjected to 3PBT. The results of the measurements are summarised in *Table 2* and *Fig. 4*.

As expected, the LWCs had the lowest compressive strength. The compressive strength of the mixture with lower body density ECA (4SD2) was significantly lower than that of the mixture with higher body density ECA (4SD1). The mixtures with andesite gravel (4S8A) and with limestone gravel (4S8L) had the highest compressive strength, which is well reflected in the high body density of both mixtures.

The results show that the values measured on cubes and on half prisms were close to each other. Typically, the variance of the values measured on half prisms was larger than that of the values measured on cubes. Based on the value pairs shown, the compressive strength values measured on half prisms were lower than the values measured on cubes if the latter was below 66 N/mm$^2$. Above 66 N/mm$^2$ the prisms had higher compressive strength.

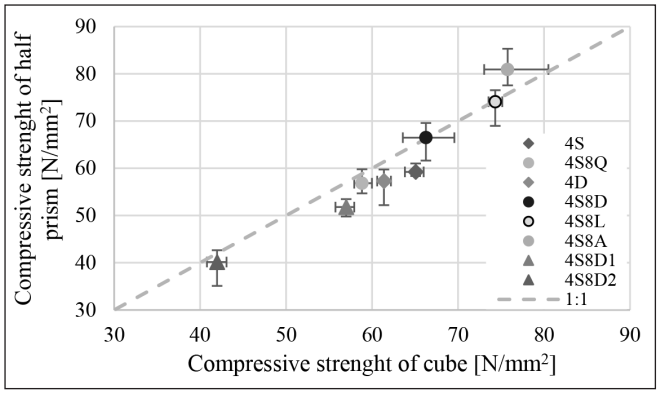


**Fig. 4:** Compressive strengths of the mixtures

## 3.3 Flexural tensile strength

From the data measured during the notched 3PBTs the flexural tensile strength of the mixture could also be directly calculated by using the following formula:

$$f_{ct,fl} = \frac{3FS}{2bh^2} \; (EN\ 14651{:}2005{+}A1,\ 2007) \qquad (1)$$

where: $f_{ct,fl}$ flexural tensile strength [N/mm$^2$],
F the force of rupture [N]
S loading span (200 mm),
b width of specimen (70 mm),
h specimen's height above the notch (57.5 mm).

The flexural tensile strength values calculated from the data measured during the notched 3PBTs are summarised in *Table 2*.

The *fib* Model Code 2010 provides a formula for the calculation of the pure tensile strength of concrete, which can be converted to flexural tensile strength by a factor depending on the width of the specimen ($\alpha_{fl}$). The formula is as follows, if the concrete strength class is higher than C50/60:

$$f_{ctm,fl} = \frac{2.12 * \ln(1+0.1(f_{ck}+\Delta f))}{\alpha_{fl}} \; (fib\ MC2010,\ 2013) \qquad (2)$$

$$\alpha_{fl} = \frac{0.06b^{0,7}}{1+0.06b^{0,7}} \; (fib\ MC2010,\ 2013) \qquad (3)$$

where: $f_{ctm,fl}$ mean flexural tensile strength [N/mm$^2$],
$f_{ck}$ characteristic compressive strength [N/mm$^2$],
$\Delta f$ 8 N/mm$^2$,
b width of specimen (70 mm).

It can be seen in the formula (Eq. 2) that 8 N/mm$^2$ is added to the characteristic value of the compressive strength of the concrete, which will thus correspond to the mean compressive strength.

In the case of LWC, the recommended relation also takes into account the body density of the concrete:

**Table 2.** Average values of measured non-mechanical and mechanical properties of the mixtures (each value is the average of 3 or 4 measurements)

| Mixture | Dry body density [kg/m$^3$] | Moisture content [%] | Apparent porosity [%] | Compressive strength [N/mm$^2$] | | Flexural tensile strength [N/mm$^2$] | Modulus of elasticity [N/mm$^2$] | Fracture energy [N/m] |
|---|---|---|---|---|---|---|---|---|
| | | | | cube | half prism | | | |
| 4S | 2090.4 | 5.67 | 16.12 | 65.06 | 59.23 | 4.41 | 20432 | 116.05 |
| 4S8Q | 2230.4 | 3.20 | 13.16 | 58.82 | 56.84 | 5.82 | 23661 | 180.10 |
| 4D | 2139.1 | 4.17 | 18.31 | 61.37 | 57.30 | 4.42 | 20172 | 92.81 |
| 4S8D | 2301.9 | 2.60 | 11.27 | 66.26 | 66.47 | 9.02 | 30950 | 146.32 |
| 4S8L | 2302.6 | 2.39 | 10.21 | 74.32 | 74.08 | 8.91 | 35579 | 121.10 |
| 4S8A | 2260.6 | 3.21 | 11.62 | 75.77 | 80.91 | 8.77 | 30453 | 158.12 |
| 4S8D1 | 1764.8 | 5.05 | 16.59 | 56.98 | 51.78 | 2.45 | 10442 | 80.16 |
| 4S8D2 | 1715.3 | 5.34 | 17.23 | 41.96 | 40.15 | 2.21 | 8460 | 95.11 |

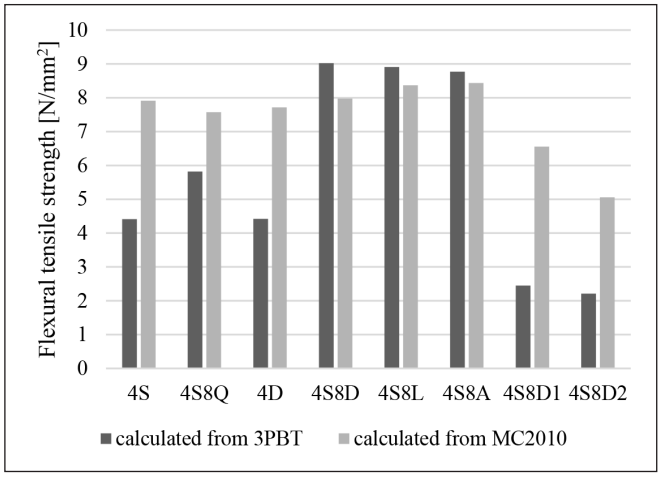


**Fig. 5:** Flexural tensile strength of the mixtures

$$f_{lctm,fl} = \frac{\mu_l * 0.3(f_{ck})^{2/3}}{\alpha_{fl}} \text{ (fib MC2010, 2013)} \quad (4)$$

$$\mu_l = (0.4 + 0.6\frac{\rho}{2200}) \text{ (fib MC2010, 2013)} \quad (5)$$

where: $f_{lctm,fl}$ mean tensile strength of LWC [N/mm²],
$f_{ck}$ characteristic compressive strength [N/mm²],
$\alpha_{fl}$ from Eq. 3,
ρ oven-dry density of the lightweight aggregate concrete [kg/m³].

The values calculated from the data measured during the notched 3PBTs and the flexural tensile strength values obtained from the previously presented formulae of the Model Code are compared in *Fig. 5.*

The results in *Fig. 5* show that the flexural tensile strength values directly calculated by 3PBT and by the compressive strength were close in case of crushed stone aggregate concretes (4S8D, 4S8L, 4S8A), where the difference was only 3-10%. In these cases, the flexural-tensile strength values directly calculated by 3PBT exceeded the ones calculated by compressive strength, so the formulas of the *fib* Model Code 2010 gave a safe approximation. In other cases, the values directly calculated by 3PBT were overestimated by the formulae of the Model Code: in the case of concrete with quartz gravel aggregate (4S8Q) and the two mixtures with 0/4 mm fractions only (4S, 4D), the difference was 30-80%. In case of LWCs, the difference of values calculated by 3PBT and using the compressive strength was even more significant and could reach 130-170%. It is important to note that the formulas proposed by the *fib* Model Code 2010 do not correspond to bending tests performed on notched specimens. In case of notches, stress concentrations may change the behaviour of the material.

## 3.4 Modulus of elasticity

From the data measured during the notched 3PBTs, the modulus of elasticity of the mixture could also be directly calculated by using the following formula:

$$E = \frac{6SaV_1(a/H)}{C_i H^2 b} \text{ (Surendra, 1990)} \quad (6)$$

$$V_1\left(\frac{a}{H}\right) = 0.76 - 2.28\left(\frac{a}{H}\right) + 3.87\left(\frac{a}{H}\right)^2 - 2.04\left(\frac{a}{H}\right)^3 + \frac{0.66}{(1-(\frac{a}{H}))^2}$$

(*Tada, Paris, and Irwin, 2000*) (7)

where: E modulus of elasticity [N/mm²],
S loading span (200 mm),
a height of the notch (12.5 mm),
$C_i$ the initial compliance calculated from the load-CMOD curve [mN⁻¹]
H height of specimen (70 mm),
b width of specimen (70 mm).

The $V_1(a/H)$ is the geometric function, which describes the relationship between the dimensions of the test specimen and the notch. The coefficient $C_i$ in the formula takes into account the initial slope of the force-CMOD curve, which was determined by fitting a line to 40% of the force of rupture. The calculated values of the modulus of elasticity are summarised in *Table 2*.

The *fib* Model Code 2010 also uses the compressive strength of concrete to determine the modulus of elasticity by the following formula:

$$E_c = E_{c0}\alpha_E(\frac{f_{cm}}{10})^{1/3} \text{ (fib MC2010, 2013)} \quad (8)$$

where: $E_c$ mean modulus of elasticity [N/mm²],
$E_{c0}$ 21.5*10³ N/mm²,
$f_{cm}$ mean compressive strength [N/mm²]
$\alpha_E$ reduction factor depending on the aggregate type.

In case of LWC, the previously presented equation (Eq. 8) is modified by a multiplication factor depending on the density of the mixture:

$$E_{lc} = \mu_E E_c \text{ (fib MC2010, 2013)} \quad (9)$$

$$\mu_E = (\frac{\rho}{2200})^2 \text{ (fib MC2010, 2013)} \quad (10)$$

where: $E_c$ calculated from Eq. 8
ρ oven-dry density of the lightweight aggregate concrete [kg/m³].

The modulus of elasticity values calculated by the results of 3PBT and the formulas of the *fib* Model Code 2010 are compared in *Fig. 6.* It can be seen that the best agreement between the results of the two calculation methods occurred in the case of crushed stone aggregate concretes. For the other mixtures, the difference was significant (95-150%). It is important to note that in the case of a notched specimen, stress concentration can occur, which can change the behaviour of the material, even the elastic behaviour of the concrete in the zone around the crack tip. Therefore, in case of lightweight aggregate and small aggregate size ($d_{max}$=4 mm), during the determination of the modulus of elasticity, it is recommended to treat the results obtained from 3PBT with caution, and rather to determine the modulus of elasticity by a standard test setup.

**Fig. 6:** Modulus of elasticity

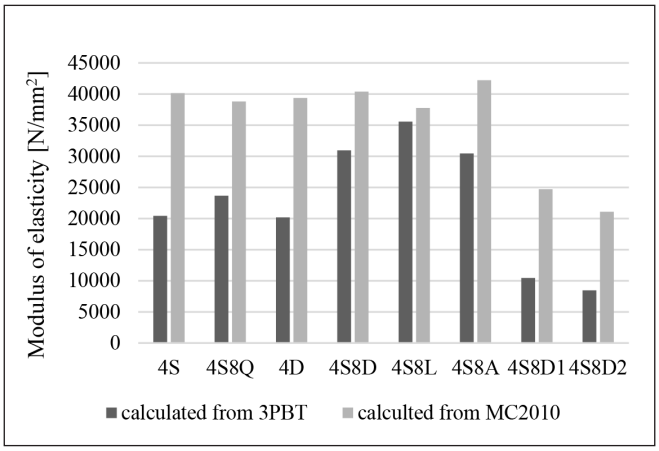

## 3.5 Fracture energy

During the research, the fracture energy was determined by the following formula

$$G_F = \frac{0.75W_0 + 0.75\left(\frac{S}{L}m\right)g * CMOD_c}{b * h} \text{ (JCI-S-001-2003, 2003)} \quad (11)$$

where $G_F$ fracture energy [N/m],
$W_0$ area below the force-CMOD curve up to rupture of the specimen [Nm],
S loading span (200 mm),
L total length of specimen (250 mm),
m mass of specimen [kg],
g gravitational acceleration (9.807 m/s$^2$),
$CMOD_c$ crack mouth opening displacement at the time of rupture [mm],
b width of specimen (70 mm),
h specimen height above the notch (57.5 mm).

The applied formula also takes into account the effect of the gravitational force acting on the specimen. Due to the test setup, the crack opening was affected not only by the loading itself but also by the self-weight of the specimen. Consequently, if the crack opening was in the critical phase, the self-weight itself could cause failure, therefore the total fracture energy could not be measured by the setup. Thus, correction by gravitational force was also required during the calculation. The average of the fracture energy values is summarised in *Table 2*.

The *fib* Model Code 2010 determines the fracture energy for NC from the average compressive strength of the concrete with the following formula:

$$G_F = 73 f_{cm}^{0.18} \text{ (fib MC2010, 2013)} \quad (12)$$

where: $G_F$ fracture energy [N/m],
$f_{cm}$ compressive strength [N/mm$^2$].

In case of LWC, another formula is used, where the average tensile strength of the concrete is included:

$$G_{F,l} = G_{f0A} + 16 f_{lctm} \text{ (fib MC2010, 2013)} \quad (13)$$

where: $G_{F,l}$ fracture energy of LWC [N/m],
$G_{F,0A}$ 24 N/m for LWC with normal weight sand
$f_{lctm}$ tensile strength of LWC [N/mm$^2$].

Previously, the formula of Model Code 1990 (*CEB-FIP, 1993*) also used the mean compressive strength of concrete, but also took into account the maximum aggregate size of the aggregate. However, this relationship corresponded only to NCs:

$$G_F = G_{F0}(f_{cm}/f_{cm0})^{0.7} \text{ (CEB-FIP, 1993)} \quad (14)$$

where: $G_F$ fracture energy [N/m],
$G_{F0}$ 0,025 N/mm, in case of 8 mm maximum aggregate size,
$f_{cm}$ compressive strength [N/mm$^2$],
$f_{cm0}$ 10 N/mm$^2$.

The fracture energy calculated by the previous formulae (Eqs. 11-14) is summarised in *Fig.* 7.

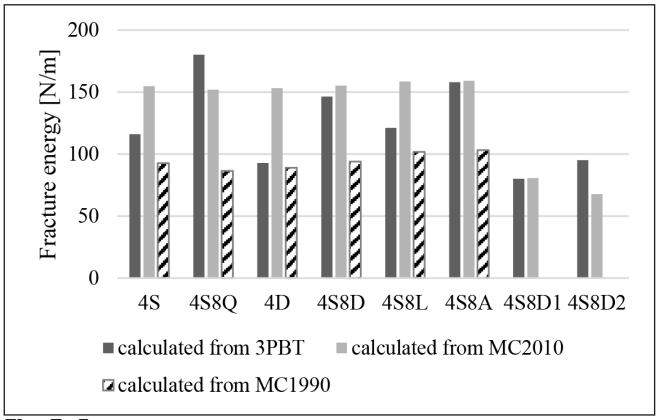


**Fig. 7:** Fracture energy

Based on the results, it can be said that the fracture energy values calculated by the formula of the Model Code 1990 (Eq. 14.) were close to the values directly calculated by 3PBT result, in case of mixtures with $d_{max}$ =4 mm (the difference was 4-20%), but significantly underestimated them in case of mixtures with $d_{max}$=8 mm (the difference was 30-50%). The formulas of the *fib* Model Code 2010, on the other hand, overestimated the fracture energy of mixtures with $d_{max}$=4 mm compared to the values directly calculated by 3PBT (the difference was 35-65%), but gave a good approximation for mixture with $d_{max}$=8 mm, even for LWCs (the difference was 0.5-25%).

## 3.6 Fracture energy as a function of compressive strength of half prisms

During the research, compressive strength was also measured on half prisms taken from the prisms previously subjected to 3PBT. The relationship between this compressive strength and thefracture energy is shown in *Fig. 8.*

To describe the relationship between the fracture energy and the compressive strength measured on half prisms, I used the equation of the Model Code 2010 (Eq. 12.) and changed only its coefficients. The measurement results were divided into three groups: NCs with $d_{max}$=4 mm, NCs with $d_{max}$ =8 mm, LWCs. Equations of the curves fitted to the results are:

$$G_{F,NC,8} = 71.7 f_{cm,0.5prism}^{0.18} \quad (15)$$

**Fig. 8:** Fracture energy as a function of compressive strength of half prisms

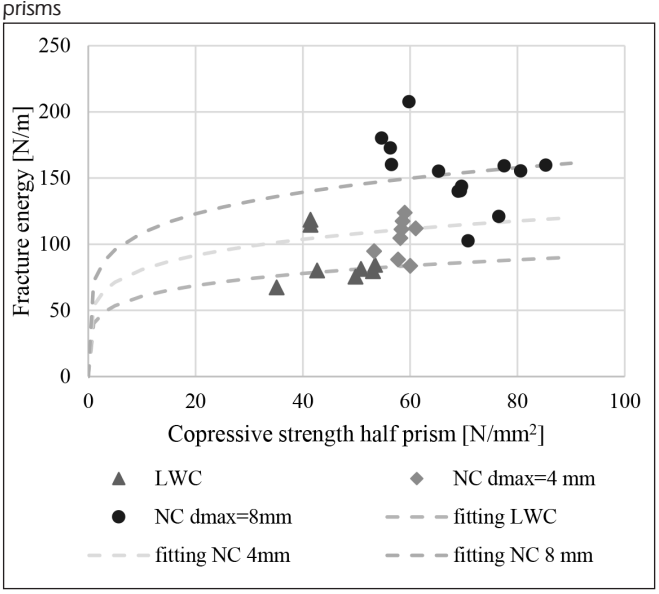

$$G_{F,NC,4} = 53.4 f_{cm,0.5prism}^{0.18} \quad (16)$$

$$G_{F,LWC} = 40.1 f_{cm,0.5prism}^{0.18} \quad (17)$$

where: $G_{F,I}$ fracture energy [N/m],
$f_{cm,0.5prism}$ compressive strength of half prism [N/mm$^2$].

From the relationship between the measured results and the curves fitted to the results, it can be seen that the *fib* Model Code 2010 formula (Eq. 12.) can be used for NCs with $d_{max}$=8 mm, if compressive strength measured on half-beams is used instead of compressive strength measured on cubes (coefficient in the original formula is 73; in the case of the curve fitted to the measured value is 71.7). On the other hand, the original formula (Eq. 13.) overestimated the values measured on NCs with $d_{max}$ =4 mm and on LWCs. In these cases, coefficients of the original formula should be changed to 53.4 for NCs with $d_{max}$=4 mm and to 40.1 for LWCs.

# 4. CONCLUSIONS

The aim of this paper was to present the calculation methods of the mechanical properties that can be determined from the results of notched 3PBTs. Seven mixtures with different types of aggregates were used (quartz, dolomite, limestone, andesite, expanded clay). To validate the obtained results, I compared the parameters determined from the 3PBTs with the formulas of the *fib* Model Code 2010 (*fib MC2010*, *2013*). Based on the results of the tests, the following can be stated:

- The compressive strength of the concrete mixtures was determined by using two types of specimens: cubes with the size of 150x150x150 mm and half prisms previously subjected to 3PBT. The results show that the individual values measured on cubes and on half prisms were close to each other. Typically, the variance of the values measured on half prisms was larger than that of the values measured on cubes. Based on the value pairs shown, the compressive strength values measured on half prisms were lower than the values measured on cubes if the latter was below 66 N/mm$^2$. Above 66 N/mm$^2$ the prisms had higher compressive strength.
- The results showed that the flexural tensile strength values directly calculated by 3PBT and by the compressive strength were close in case of crushed stone aggregate concretes (4S8D, 4S8L, 4S8A), where the difference was 3-10%. In other cases, the values directly calculated by 3PBT were overestimated by the formulae of the Model Code. In case of LWCs, the difference could reach 130-170%. It is important to note that the formulas proposed by the *fib* Model Code 2010 do not correspond to bending tests performed on notched specimens. In case of notches, stress concentrations may change the behaviour of the material. This can be the reason why in case of concrete mixtures which were more sensitive to tension ($d_{max}$=4 mm, or LWC), the results directly calculated by 3PBT were significantly lower than the results calculated by the *fib* Model Code 2010.
- In case of the results of the modulus of elasticity, the best agreement between the results of the two calculation methods occurred in the case of crushed stone aggregate concretes. For the other mixtures, the difference was significant (95-150%). It is important to note again that in case of a notched specimen, stress concentration can occur, which can change the behaviour of the material, even the elastic behaviour of the concrete in the zone around the crack tip. Therefore, in case of lightweight aggregate and small aggregate size ($d_{max}$=4 mm), during the determination of the modulus of elasticity, it is recommended to treat the results obtained from 3PBT with caution, and rather to determine the modulus of elasticity by a standard test setup.
- Based on the results, the fracture energy values calculated by the formula of the Model Code 1990 were close to the values directly calculated by 3PBT result, in case of mixtures with $d_{max}$ =4 mm (the difference was 4-20%), but significantly underestimated them in case of mixtures with $d_{max}$=8 mm (the difference was 30-50%). The formulas of the *fib* Model Code 2010, on the other hand, overestimated the fracture energy of mixtures with $d_{max}$=4 mm compared to the values directly calculated by 3PBT (the difference was 35-65%), but gave a good approximation for mixture with $d_{max}$=8 mm, even for LWCs (the difference was 0.5-25%).
- During the research, I also performed compressive strength tests on half prisms previously used for notched 3PBT. Thus, compressive strength values measured on half prisms could be associated with fracture energy values. From the relationship between the measured results and the curves fitted to the results, it could be seen that the *fib* Model Code 2010 formula could be used well for NCs with $d_{max}$=8 mm. Compressive strength measured on a half prism was used, and the coefficient in the formula was slightly modified. However, the formula of the Model Code overestimated the values measured on NCs with $d_{max}$=4 mm and on LWC mixtures. In these cases, the coefficient of the original formula had to be significantly modified.

# 5. ACKNOWLEDGEMENT

The authors wish to thank Dr. Éva Lublóy, Dr. Salem Georges Nehme and Dr. Miklós Gálos for providing the necessary materials and for the professional advice. Thanks to Balázs Burai and Viktória Rónaky for their help in the laboratory measurements. Authors acknowledge the support by the Hungarian Research Grant NVKP_16-1-2016-0019 "Development of concrete products with improved resistance to chemical corrosion, fire or freeze-thaw". This research was supported by the ÚNKP-20-4 New National Excellence Program of The Ministry for Innovation and Technology from The Source of The National Research, Development and Innovation Fund.

# 6. REFERENCES

Alimrani, N. S., and Balazs, G. L. (2020). Investigations of direct shear of one-year old SFRC after exposed to elevated temperatures. *Construction and Building Materials*, *254*, 119308. https://doi.org/10.1016/j.conbuildmat.2020.119308

Bažant, Z. P., and Planas, J. (1997). *Fracture and Size Effect in Concrete and Other Quasibrittle Materials*. CRC Press. ISBN: 0-8493-8284-X

CEB-FIP. (1993). *MODEL CODE 1990*. Thomas Telford Publishing. ISBN: 0 7277 1696 4

EN 12350-5:2019. (2019). *Testing fresh concrete - Part 5: Flow table test*.

EN 12390-3:2019. (2019). *Testing hardened concrete – Part 3: Compressive strength of test specimens*.

EN 14651:2005+A1. (2007). *Test method for metallic fibre concrete - Measuring the flexural tensile strength (limit of proportionality (LOP), residual)*.

EN 1936:2007. (2007). *Natural stone test methods - Determination of real density and apparent density, and of total and open porosity*.
Fehérvári, S., Gálos, M., and Nehme, S. G. (2010a). Determination of KIIC stress intensity factor on new shape concrete specimens. *Concrete Structures*, *11*, 53–60.
Fehérvári, S., Gálos, M., and Nehme, S. G. (2010b). Determination of KIIC stress intensity factor on new shape concrete specimens (Part II). *Epitoanyag-Journal of Silicate Based and Composite Materials*, *62*(2), 34–38. https://doi.org/10.14382/epitoanyag-jsbcm.2010.7
***fib*** BULLETIN 8. (2000). *Lightweight Aggregate Concrete - Recommended extensions to Model, Code 90 - Case studies*. Stuttgart, Germany.
***fib*** MC2010 (2013). *MODEL CODE 2010*. Berlin, Germany: Ernst&Sohn. ISBN: 978-3-433-03061-5
Griffits, A. A. (1921). VI. The phenomena of rupture and flow in solids. *Philosophical Transactions of the Royal Society of London. Series A, Containing Papers of a Mathematical or Physical Character*, *4*(1), 9–14. https://doi.org/10.1098/RSTA.1921.0006
Hillerborg, A. (1985). The theoretical basis of a method to determine the fracture energy GF of concrete. *Materials and Structures*, *18*, 291–296. https://doi.org/10.1007/BF02472919
Hillerborg, A., Modéer, M., and Petersson, P. E. (1976). Analysis of crack formation and crack growth in concrete by means of fracture mechanics and finite elements. *Cement and Concrete Research*, *6*(6), 773–781. https://doi.org/10.1016/0008-8846(76)90007-7
Irwin, G. R. (1957). Analysis of Stresses and Strains Near the End of a Crack Traversing a Plate. *Journal of Applied Mechanics*, *24*(3), 361–364. https://doi.org/10.1115/1.4011547
JCI-S-001-2003. (2003). *Method of test for fracture energy of concrete by use of notched beam*.
Kaplan, M. (1961). Crack propagation and the fracture of concrete. *Journal Proceedings*.
Khalilpour, S., BaniAsad, E., and Dehestani, M. (2019). A review on concrete fracture energy and effective parameters. *Cement and Concrete Research*, *120*, 294–321. https://doi.org/10.1016/J.CEMCONRES.2019.03.013
Lee, J., and Lopez, M. M. (2014). An Experimental Study on Fracture Energy of Plain Concrete. *International Journal of Concrete Structures and Materials*, *8*(2), 129–139. https://doi.org/10.1007/s40069-014-0068-1
Lublóy, É., Balázs, G. L., and Czoboly, O. (2013). Influence of particular components of concrete composition to residual compressive strength after temperature loading. In J. Biliszczuk, J. Bien, P. Hawryszków, & T. Kaminski (Eds.), *The 9th Central European Congress on Concrete Engineering* (pp. 4–6). Wroclaw, Poland.
Nemes, R., and Józsa, Z. (2006). Aspects of Mix Design of Lightweight Aggregate Concrete. *Concrete Structures*, *7*, 82–87.
Rao, A. S., and Rao, G. A. (2014). Fracture mechanics of fiber reinforced concrete: an overview. *International Journal of Engineering Innovations and Research*, *3*(4), 517.
RILEM Technical Committee 50 FMC. (1985). Draft recommendation: determination of the fracture energy of mortar and concrete by means of three-point bend test on notched beams. *RILEM Materials and Structures*, *18*(107), 407–413.
Sólyom, S., Di Benedetti, M., and Balázs, G. L. (2021). Bond of FRP bars in air-entrained concrete: Experimental and statistical study. *Construction and Building Materials*, *300*. https://doi.org/10.1016/j.conbuildmat.2021.124193
Surendra, P. S. (1990). Determination of fracture parameters (KIc and CTODc) of plain concrete using three-point bend test. *Materials and Structures*, (23), 457–460. https://doi.org/10.1007/BF02472029
Tada, H., Paris, C. P., and Irwin, G. R. (2000). *The stress analysis of cracks handbook* (Third edit). New York: The American Society of Mechanical Engineers. ISBN: 0-7918-0153-5

**Viktor Hlavička** (1987), Structural Engineer MSc, PhD, concrete technologist, fire safety engineer, Assistant Professor of Department of Construction Materials and Technologies, Budapest University of Technology and Economics. His main fields of interest are experimental investigation and modelling of fastening systems in concrete and thermally damaged concrete. He is a member of the Hungarian Group of ***fib***. email: hlavicka.viktor@emk.bme.hu

# MODERN NUMERICAL MODELING OF REINFORCED CONCRETE STRUCTURES


https://doi.org/10.32970/CS.2021.1.3

Zsolt Roszevák - István Haris

*Nowadays, many computer software products are available for the numerical modeling of reinforced concrete structures; however, the accuracy of the numerical models created by the programs can only be accepted with a properly developed and verified modeling procedure. Within the framework of the present article, we present the numerical modeling possibilities of reinforced concrete structural elements and their connections through numerical models made by a modeling procedure we have built. In our studies, we also dealt with quasi-static unidirectional (horizontal and vertical) and cyclically variable direction and magnitude loads. The numerical models were created using the ATENA 3D three-dimensional nonlinear finite element software developed specifically for the study of concrete and reinforced concrete structures. In many cases, the results obtained by numerical experiments were compared with the results obtained by laboratory experiments, and some of our numerical experiments were compared with the results obtained using two-dimensional finite element software. Within the framework of this article, we would like to give a comprehensive picture of the numerical studies we have performed. We have also briefly summarized the results and experiences obtained from 3D nonlinear finite element studies.*

**Keywords:** ATENA 3D software, nonlinear finite element analysis, cast-in-situ reinforced concrete structures, prefabricated reinforced concrete structures

## 1. INTRODUCTION

Nowadays, research engineers perform numerical studies on a number of topics, as a result of which they are able to model the behavior of individual structural elements by computer. At the same time, there is a growing demand for this from practicing engineers. However, in order to verify numerical models and their results, it is essential to perform laboratory experiments by which we can support the correctness and accuracy of our numerical models. From a practical point of view, it is important that the numerical model created follows the real behavior of the structure as closely as possible. Therefore our models will become more and more detailed and thus more complex. From the point of view of modeling reinforced concrete structures, the properties of the materials and material models that can be used in the chosen finite element software cannot be neglected. We must use or apply software with which we can properly study the problem we have analyzed.

In the course of our research, we have dealt with the numerical examination of several reinforced concrete structural elements and are still dealing with them. Our goal is to produce an extensively developed and well-founded numerical modeling technique by the development of numerical models, which we can use to examine reinforced concrete structural elements and their node design in the most appropriate way in reality in the target software. During numerical model development, we perform a significant number of parameter tests, which are basically performed to cover individual structural details, nodes and complete structural elements. Taking advantage of the possibilities provided by the finite element software at the highest level, we performed hundreds of numerical runs through the optimization of the computation time and the finite element distribution through individually parameterizable material models in the software (products).

Within the framework of this article, we present the most important results achieved in the current field of research and in the course of our previous research. A significant part of the results is related to the numerical modeling procedure, but the results obtained by the numerical modeling method are also considered significant research results in the subject. Prior to our research, we conducted a comprehensive literature review, on the basis of which it can be clearly established that the numerical modeling of reinforced concrete structures is basically moving towards high-level finite element calculations. However, the sources available mostly publish laboratory experiments, which were used in only few cases to verify and develop numerical models. Numerical models are almost exclusively 2D linear (Szczecina, Winnicki, 2015, Hwang, Lee, 1999), and less frequently nonlinear (Hawileh, Rahman, Tabatabai, 2010), (Masi, Santeriero, Nigro, 2013); three-dimensional nonlinear finite element calculations are rarely found (Santeriero, Masi 2017), (Arjamadi, Yousefi, 2018). Taking all this into account, there is a growing demand in the subject for the development and application of three-dimensional nonlinear finite element models. High-level numerical studies of reinforced concrete structures, such as the structural elements and their connections discussed in this article, can by no means be considered a fully exploited

research area. Understanding the behavior of monolithic and precast reinforced concrete structures and the numerical studies of the different connection designs and the different types of reinforcement placing used in them will help to understand and describe the behavior of the given connection / structural element. Thus, with 3D nonlinear finite element software proven on the basis of real laboratory experiments, a number of structural designs that have not been tested under laboratory conditions or are difficult to handle experimentally due to their size can be examined. Within the framework of this article, we have summarized the results and experiences obtained in our numerical studies. We summarized what results could be achieved by the modeling procedure we developed during the examination of each structural element and connection.

## 2. DEVELOPMENT OF THE NUMERICAL MODELLING METHOD

The finite element models were built using the ATENA 3D nonlinear finite element software *(Figure 1(a))*. Numerical model development was basically started with the performance of quasi-static studies, and then the results and experiences of quasi-static computation were used in cyclic studies *(Figure 1(b))*. In many cases, a laboratory experiment published in the literature was available. The parameters and results provided in the publications were used in the preparation of the numerical models.

In the quasi-static numerical experiments, the material model of concrete was defined by an individually parametrized model on the basis of our previous results (Haris, Roszevák 2017, Roszevák, Haris, 2019). The reinforcement material model is specified according to the properties of the reinforcement used in the laboratory experiments and it is provided with the real stress-deformation characteristic *(Figure 2(b))*. The strength properties of the concrete and reinforcement bars have been defined according to the laboratory tests.

The relationship between the concrete and reinforcement bars *(Figure 2(d))* was calculated and defined on the basis of the CEB-FIP 1990 Model Code (*fib*-Model Code for Concrete Structures, 2010). The longitudinal bars were modeled with their real geometry and diameter, the stirrups with a closed rectangular shape other than the actual bending shape, but with their real diameter.

In our cyclic test, the material for concrete shown in *Figure 1(a)* was used. The concrete material model includes the following effects of concrete behaviour (Červenka et al., 2014): non-linear behaviour in compression including hardening and softening, reduction of compressive strength after cracking (Van Mier, 1986), fracture of concrete in tension based on nonlinear fracture mechanics (Hordijk, 1991), biaxial strength failure criterion (Kupfer et al.,1969), tension stiffening effect, reduction of shear stiffness after cracking (Kolmar, 1986) and the fixed (Červenka, 1985, Darwin & Pecknold, 1974) and rotated (Vecchio & Collins, 1986, Crisfield & Wills, 1989) crack direction. For tensile (fracture) and compressive (plastic) behavior, the software uses a smeared crack approach in concrete junction with a fracture plastic model. The rotating and fixed crack models can be used in connection with exponential softening and the Rankine tensile failure criterion. ATENA 3D adds a so-called "Unloading Factor" to model concrete behavior under cyclic loading. The "Unloading Factor" controls crack closure stiffness. The factor mainly influences the shape of the hysteresis curve; in our analyses the parameter was set to zero because this value gives the best fit to real behaviour (Červenka et al., 2014). The reinforcement is defined by cyclic properties based on the Menegotto-Pinto model (Menegotto, Pinto, 1973) *(Figure 2(c))*. In the longitudinal bars placed in the concrete elements, the effect of slipping was taken into account. However, we have set the perfect connection for the stirrups. The slip of the reinforcement bars has been taken into account: the relationship between concrete and reinforcement bars is defined by a memory bond parametrized model. We have taken the bond-slip relationship *(Figure 2(e))* in the model according to the CEB-FIP 1990 Model Code. The placing of the bars has been defined in the same way at the quasi-static tests.

For all nonlinear analyses, an iterative method (Newton-Raphson iteration method) was used to perform the iteration process. The Cholesky resolution was used to solve the state equation of the structure. In the numerical models we used

**Fig. 1:** Development of numerical modeling method (a) Structural elements, (b) Types of loading

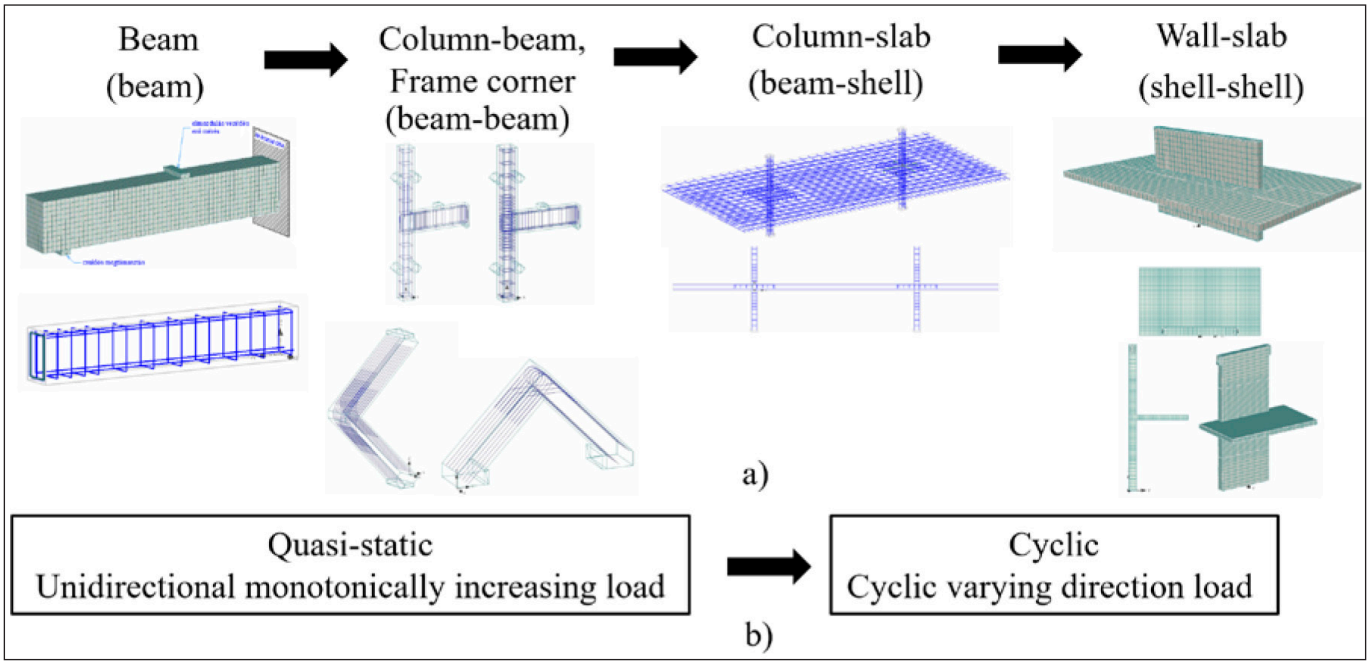

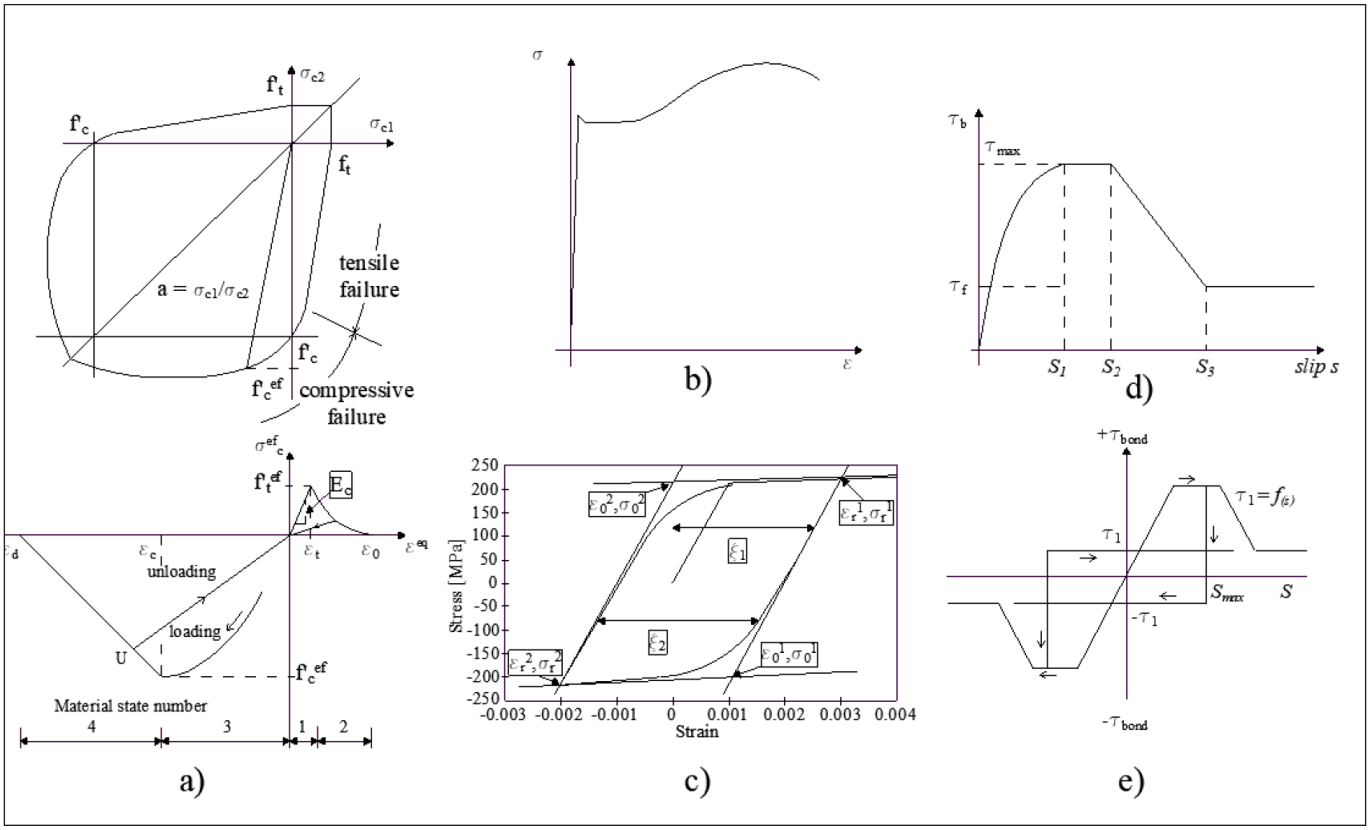


***Fig. 2:*** *Material properties: (a) concrete material model, (b) reinforcement stress-strain relationship, (c) cyclic reinforcement model, (d) bond-slip relationship (quasi-static), (e) bond-slip relationship (cyclic). From Cervenka et al., 2014*

uniformly quadratic bar functions, and we used 20-node brick elements for the concrete (Haris, Roszevák, 2017). The finite element mesh is distributed uniformly so that there are at least four finite elements within the given cross-sectional dimension (Haris, Roszevák, 2017). The choice of the mesh size of the finite elements depends, in many cases, on the size of the structural element examined and the body elements forming the node model, so in many cases, we used allocated finite elements in the connection environment.

We started our studies with laboratory and numerical experiments of simple reinforced concrete beams in order to be able to verify our numerical model on a simple (single supported) beam element and to examine each input parameter. In the next step, we modeled the beam-beam connection designs, in which the behavior of the closing and opening frame corners and beam-column connections was investigated. Afterwards, we performed the modeling of beam-shell connections, in which we also dealt with the formation of column and slab connections through the determination of substitute equivalent plate width. The final step of the present program is the relationship between shell-shell structural elements. The examination of wall and slab type relationships is an issue which we have already dealt with tangentially before, and we have made preliminary numerical models. The research is currently in the phase of conducting a large-scale, completely novel laboratory experiment of 16 specimens for wall-slab type connections, which can be used for verifying previously developed numerical models, and detailed parameter analysis can be performed.

We have carried out our research in the first place in the field of cast-in-situ reinforced concrete structures; however, the research has reached that stage and we have set up a research group to enable the performance of investigations of prefabricated reinforced concrete structural elements. In the case of prefabricated structural elements, we are currently dealing with the possibilities of modeling the relationships of structural elements and numerical studies of prestressed structural elements.

## 3. SUMMARY OF RESULTS

Numerical studies of beam-column *(Figure 3(a))* and frame corner *(Figure 3(b))* connections were performed using the 3D modeling procedure we developed for a monotonically increasing, quasi-static load *(Figure 3(c), (d))*. The numerical models were constructed with the actual concrete cross-section and reinforcement used in real international laboratory experiments found in the literature (Yap, Li, 2011; Morgan, 2000), so that the results obtained could be directly compared with each other. In the case of beam-column specimens, a very good agreement can be detected in the initial non-cracked and failure-to-failure sections. With displacement-controlled numerical experiments, the flattening behavioural phase after failure cannot be modeled by the modeling technique we use. In force-controlled numerical experiments, on the other hand, the post-failure behavioural phase can be shown *(Figure 4(a))*. It can be stated that numerical models with actual (real) reinforcement characteristics yield better results than models where the linear elastic-linear hardening reinforcement material model was used. Plastic deformations after failure can be modeled using the real rebar characteristic. The crack pattern produced by numerical tests shows a good agreement with the crack pattern recorded in the laboratory experiments *(Figure 4(b), (d))*.

For a more accurate examination of cracks, reducing the size of the finite element mesh may be a good solution; however, it increases the running time of the models almost exponentially. The "efficiency" of the applied reinforcement placing and rebar quantity can be examined numerically, and in this case the connection can be optimized for load-bearing capacity, deformability, reinforcement quantity and even costs (Roszevák, Haris, 2019). We have shown that it

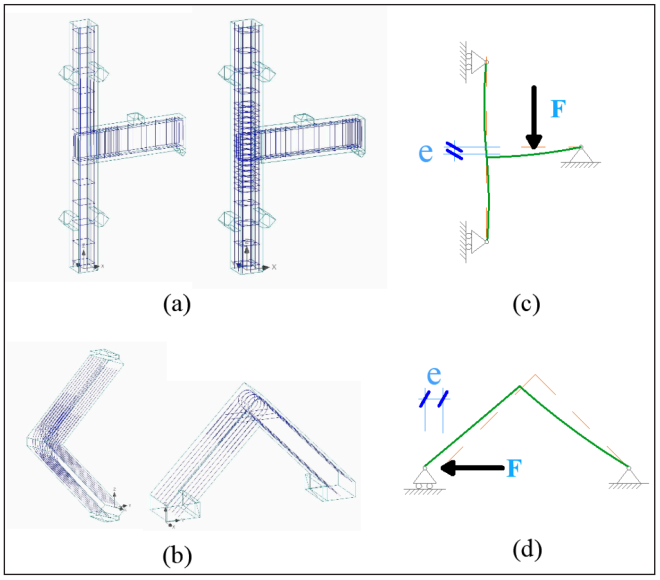


**Fig. 3:** Beam-column and frame corner connections: (a) ATENA 3D model (beam-column), (b) ATENA 3D model (frame corner), (c) static structure (beam-column), static structure (frame corner)

is possible to analyze the complex behaviour of monolithic reinforced concrete frame connections formed with the same reinforcement ratio but with different rebar placing under one-way monotonically increasing quasi-static loading instead of a very expensive series of laboratory experiments *(Figure 4(c))*.

With our improved modeling method, the real behaviour of cast-in-situ reinforced concrete beam-column connections (within a defined displacement limit) under horizontal cyclically varying directional loads *(Figure 5(a))* is extremely well-approximated by a finite element calculation within the given test range. During the individual finite element calculations, under horizontal quasi-static loads, we applied horizontal cyclically varying force loads, with which we were able to study the complex behaviour of the connections of the investigated specimens with sufficient accuracy. The connections made with the different placing patterns of reinforcement and stirrups can be modeled *(Figure 5(b), (c))*, using the modeling technique we have defined, by a nonlinear, three-dimensional finite element program within the given deformation range with sufficient accuracy to describe the behaviour (within 5-10%). To model the cyclically changing horizontal load, we compared the numerical models *(Figure 6)* produced with the improved version of the previously defined modeling technique, also with laboratory experiments found in the international literature (Masi, Santeriero, Nigro 2013). With the modeling technique developed, it is also possible to study the behavior of new, but even of existing cast-in-situ reinforced concrete structural joints against seismic, cyclic horizontal loads up to the deformation limits set in domestic and international standards (Roszevák, Haris, 2019).

The modeling method developed is also suitable for the analysis of point-supported flat slabs for vertical and horizontal loads. Using the verified numerical model, we showed in a geometric arrangement identical to the laboratory experiments that a linear computational framework model,

**Fig. 4:** Results of the numerical analysis: (a) force-displacement diagram (beam-column), (b) crack patterns (beam-column), (c) force-displacement diagram (frame corner), crack patterns (frame corner)

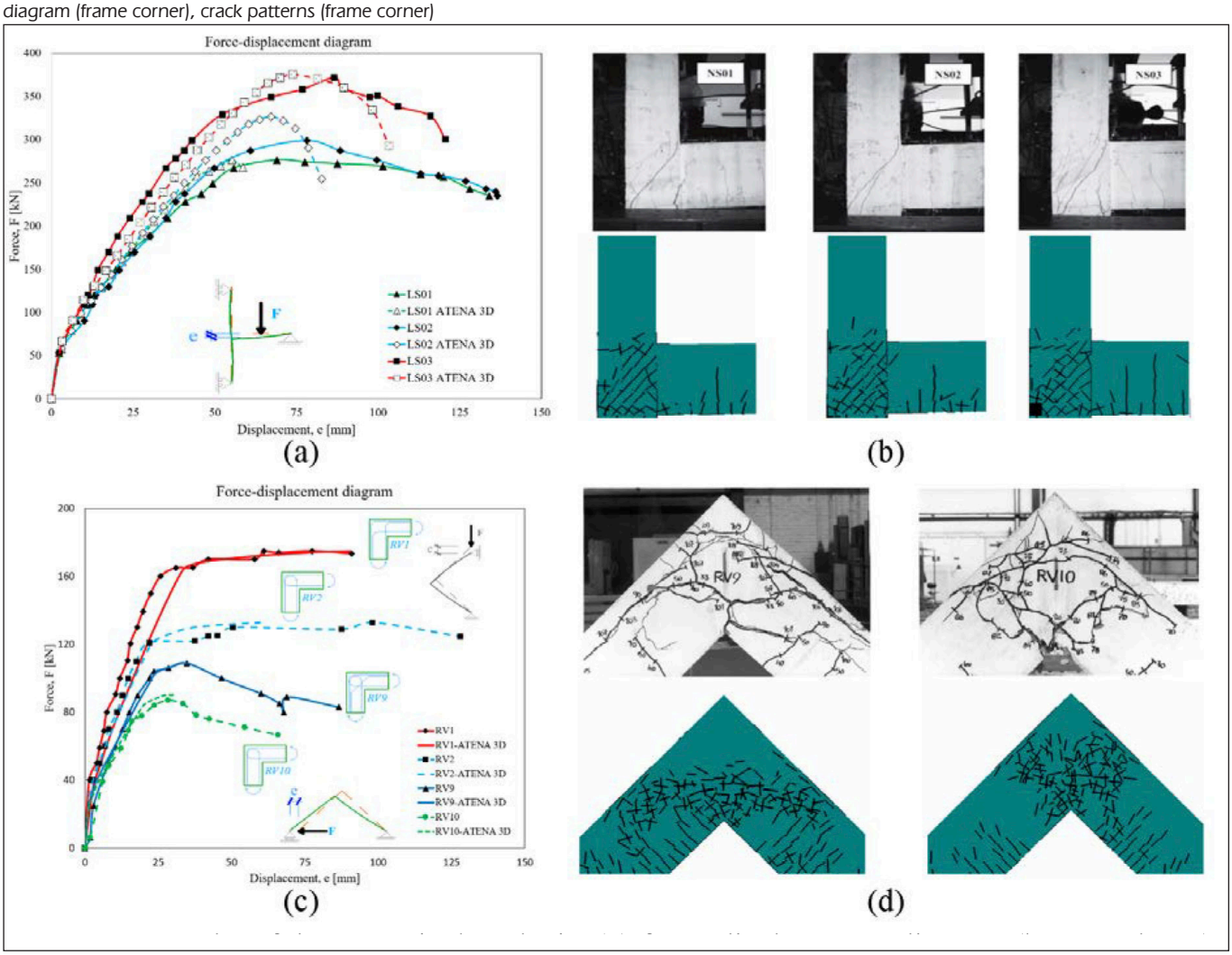

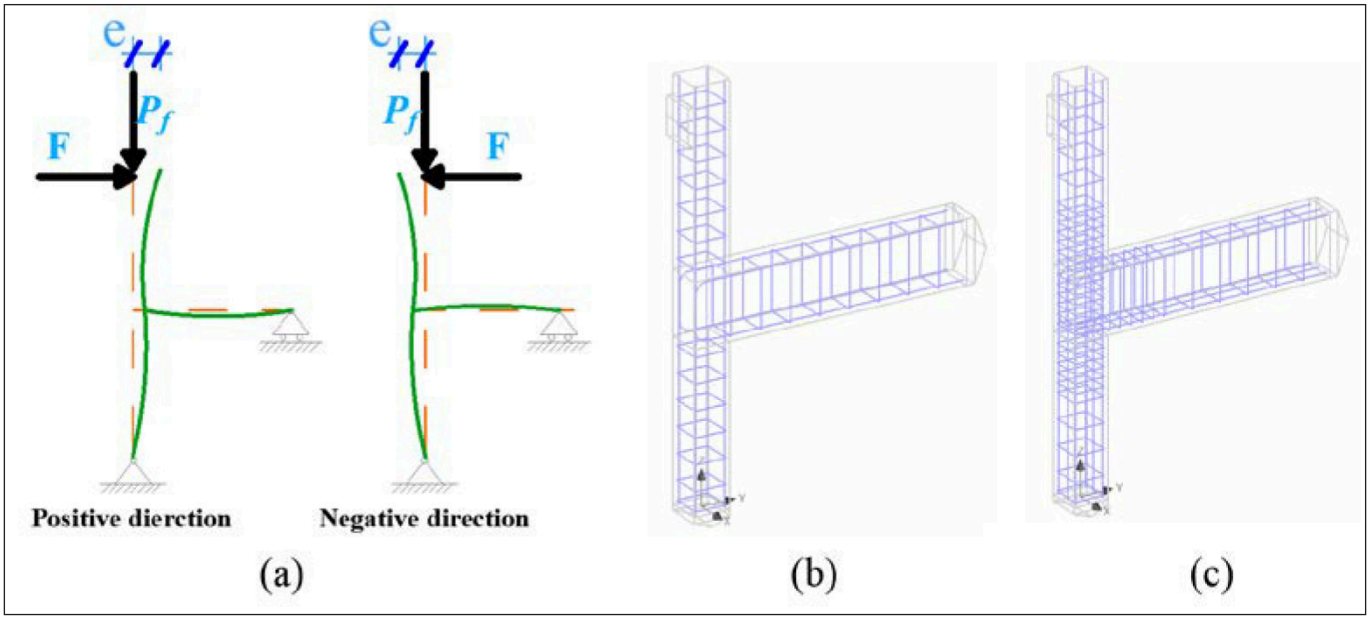


**Fig. 5:** Beam-column connections: (a) static structure and loading, (b) ATENA 3D model (NE FB), (c) ATENA 3D model (Z4 RB)

approximating the results of nonlinear virtual experiments describing the behavior of column-supported flat slabs, can be generated using an equivalent beam width method. We have shown that the modeling method is suitable for a more accurate description of real structural behavioural stages with significant plastic deformations. By combining and geometrically extending the nonlinear numerical results and the much simpler but easier-to-use linearly flexible computational model, we have shown that a function of one or two variables suitable for recording the replacement plate width can be produced *(Figure 7.)*. It can specify the value of replacement reduction factors in proportion to the thickness of the slab, the cross-sectional size of the column, raster distribution, and the desired force-displacement (Roszevák, Bodó, Haris, 2019).

Using the results and experiences so far, we have also started to conduct research in a new direction. We examined the behaviour of connections (beam-column and column-cup-foundation) in a simple prefabricated reinforced concrete frame structure and the modeling capabilities of each connection (Roszevák, Haris, 2021). Basically, we made separate joint models of the prefabricated frame; however, using the results of the joint models, we also created a complex frame model *(Figure 8)*. The results obtained using

**Fig. 6:** Comparison of numerical and experimental results

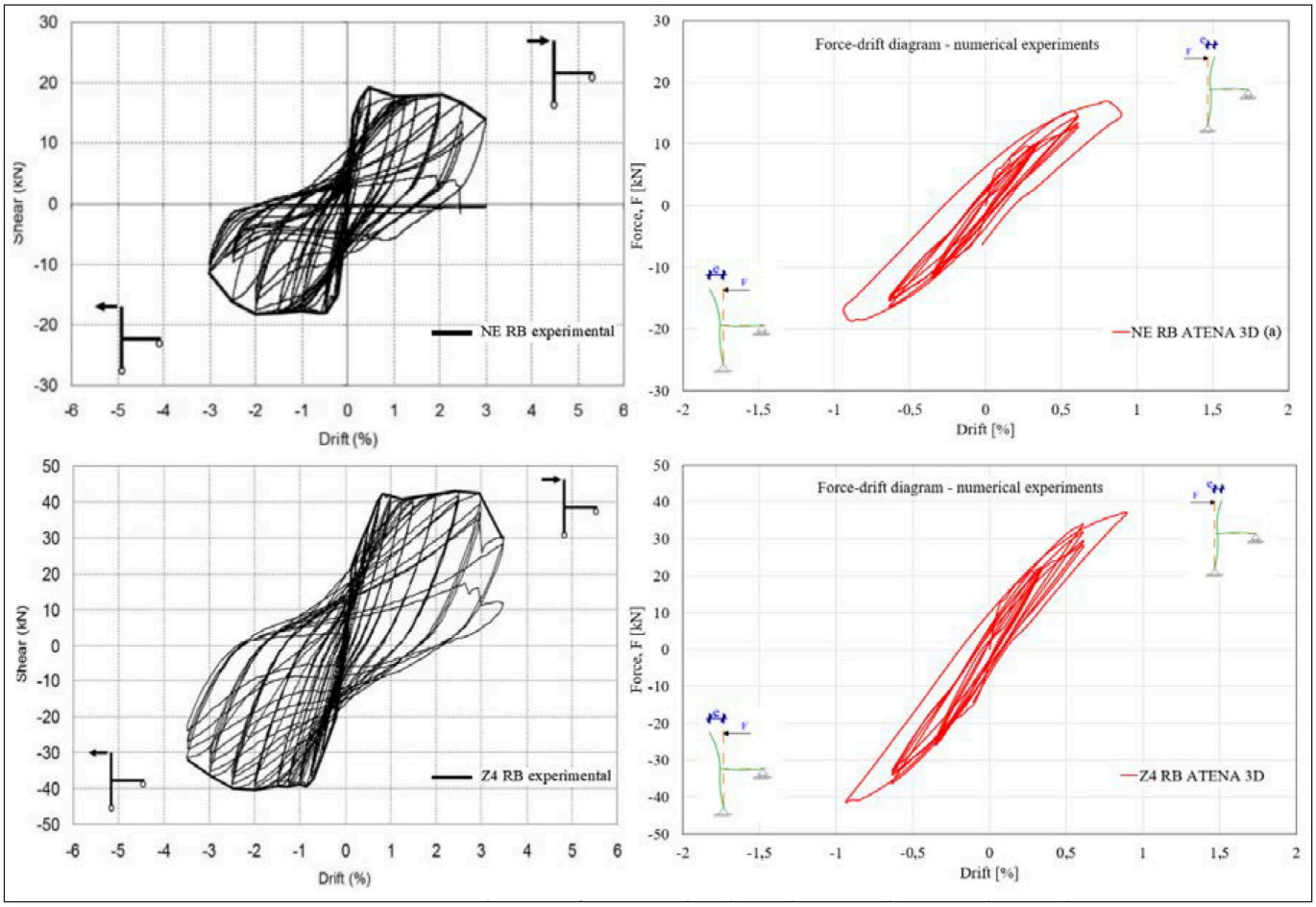

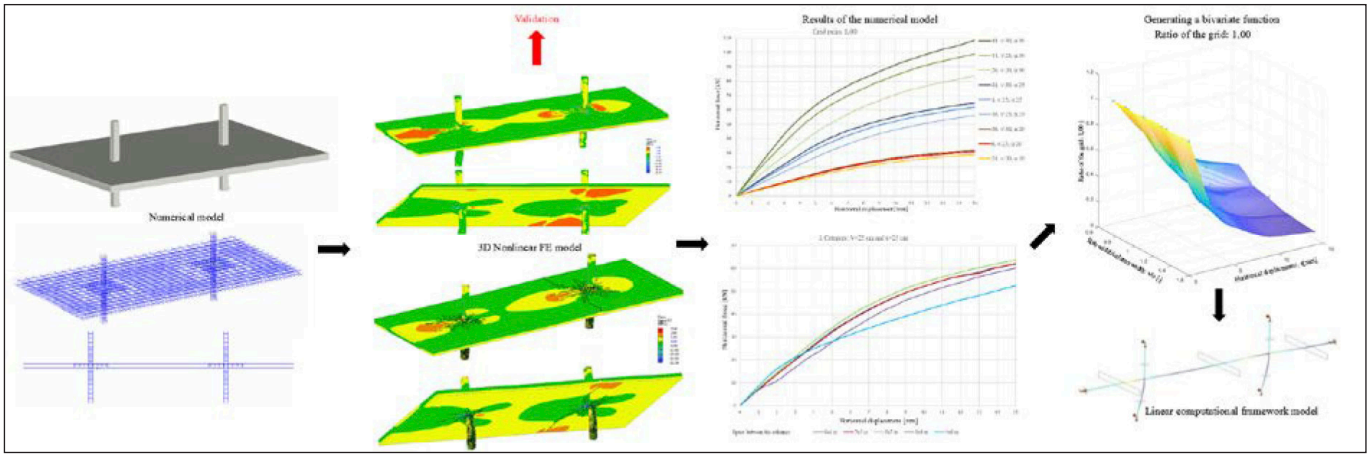


**Fig. 7:** Flowchart of the equivalent replacement framework model

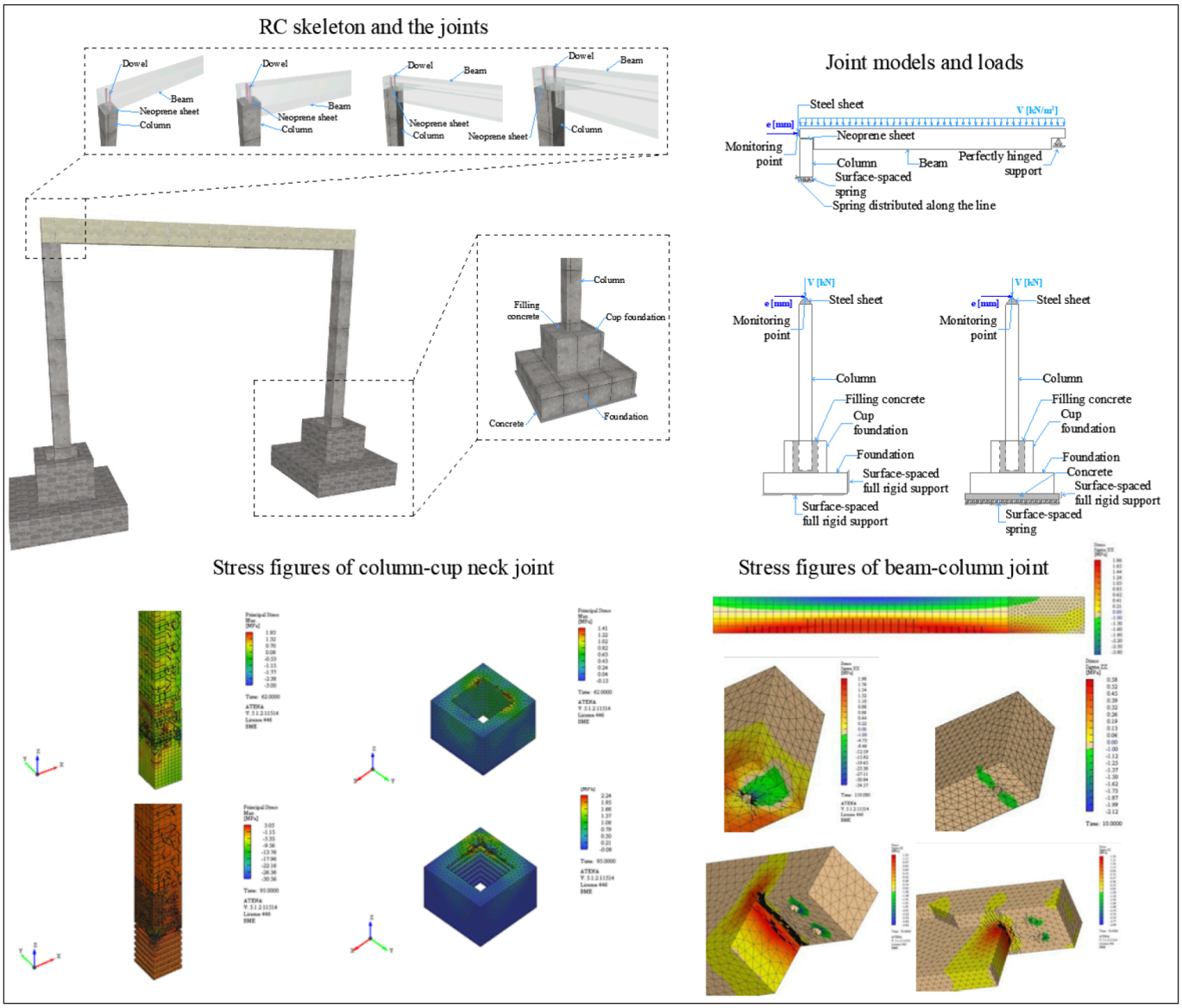


**Fig. 8:** Analysis of prefabricated RC skeleton

simple two-dimensional (linear and nonlinear) finite element models were compared with the results obtained using 3D nonlinear finite element joint models.

In the case of cup-foundation joints, we investigated the effect of the ribbed design of the lower part of the column, the possibility of modeling the shrinkage of the filling concrete between the cup neck and the column and we also started to investigate the possibilities of supporting the cast-in-situ reinforced concrete foundation. In the case of column-beam joints, we investigated the effect of the diameter and the number of rebar dowels on the behaviour of the joint. We also analyzed the effect of neoprene plate dimensions and the modeling possibilities of the filling mortar around the dowel and of the types of the beam's cross-section. Finally, we examined the effect of each joint design on the behavior of the global framework.

We also performed the tests of cast-in-situ reinforced concrete (stiffening) wall and slab connections (Roszevák, Haris, 2017) with unidirectional monotonically increasing quasi-static *(Figure 9)* and cyclically varying loads using the modeling procedure defined in our previously verified numerical models. Based on our results, it can be stated

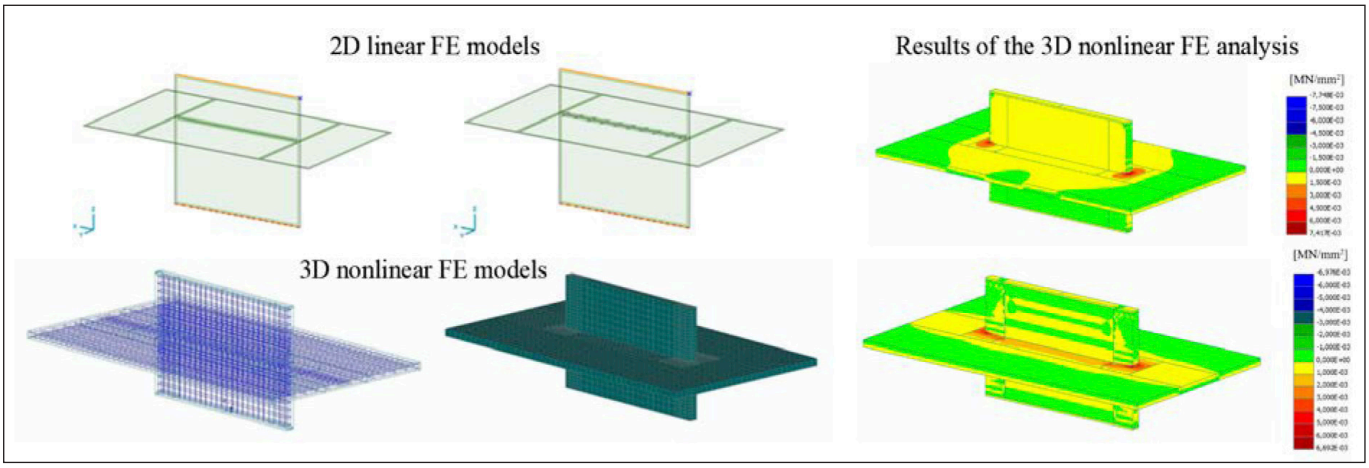


**Fig. 9:** *Numerical models for wall-slab connections (quasi-static vertical loading)*

that instead of the numerically infinitely large support at the bottom and top of the wall, spring support is more suitable for the study than in the case of the models made for cyclically changing direction load and unidirectional monotonically increasing load. By reducing spring support in proportion to stiffness, the finite element calculation does not result in a numerical error as in the case of "infinitely large" support. The reinforcing bars are spliced in the design of our test connections: side-by-side reinforcing bars must be placed in the cross-section of the joint at least at the same axial distance as a quarter of the diameter of the bars, so that the finite element calculation does not yet result in an error.

Recently and nowadays, cast-in-situ reinforced concrete stiffening walls are always tested under laboratory conditions on simplified experimental elements loaded in plane with specifically horizontal loads, without the associated structures. In the case of horizontal effects of cyclically varying direction and magnitude, descriptions of structural behavior should come to the fore even more in order to get a detailed understanding of the stiffness conditions of the cast-in-situ reinforced concrete wall-slab connection. Our goal is to investigate a unique element of a general torsional stiffening system, to accurately describe the structural behavior of a wall-slab connection both by numerical modeling and by the targeted laboratory testing of structural connections.

A series of 16 test specimens were designed to examine the structural elements *(Figure 10)*. The aim of the laboratory experiments is to study the actual design of the wall-slab connections and the effect of different modes of reinforcement placing on the joints and their effect on load-bearing capacity, stiffness, crack pattern and deformations. According to the results it is possible to verify high complexity and sophisticated three-dimensional nonlinear finite element models. Another goal is to describe the stiffness of the stiffening walls and the relationship between the stiffening walls and the slabs more accurately and efficiently, to supplement and/or clarify the designing formulas that can be used in everyday engineering practice, and to formulate structural design guidelines and recommendations.

## 4. CONCLUSIONS

In the field of cast-in-situ reinforced concrete structures, we performed several numerical studies, which were created with the modeling procedure we developed. In many cases, the performed numerical analyses were compared with the mostly international laboratory experiments found in

**Fig. 10:** *Numerical models and laboratory experiments for wall-slab connections (quasi-static vertical loading and cyclic variable horizontal loading)*

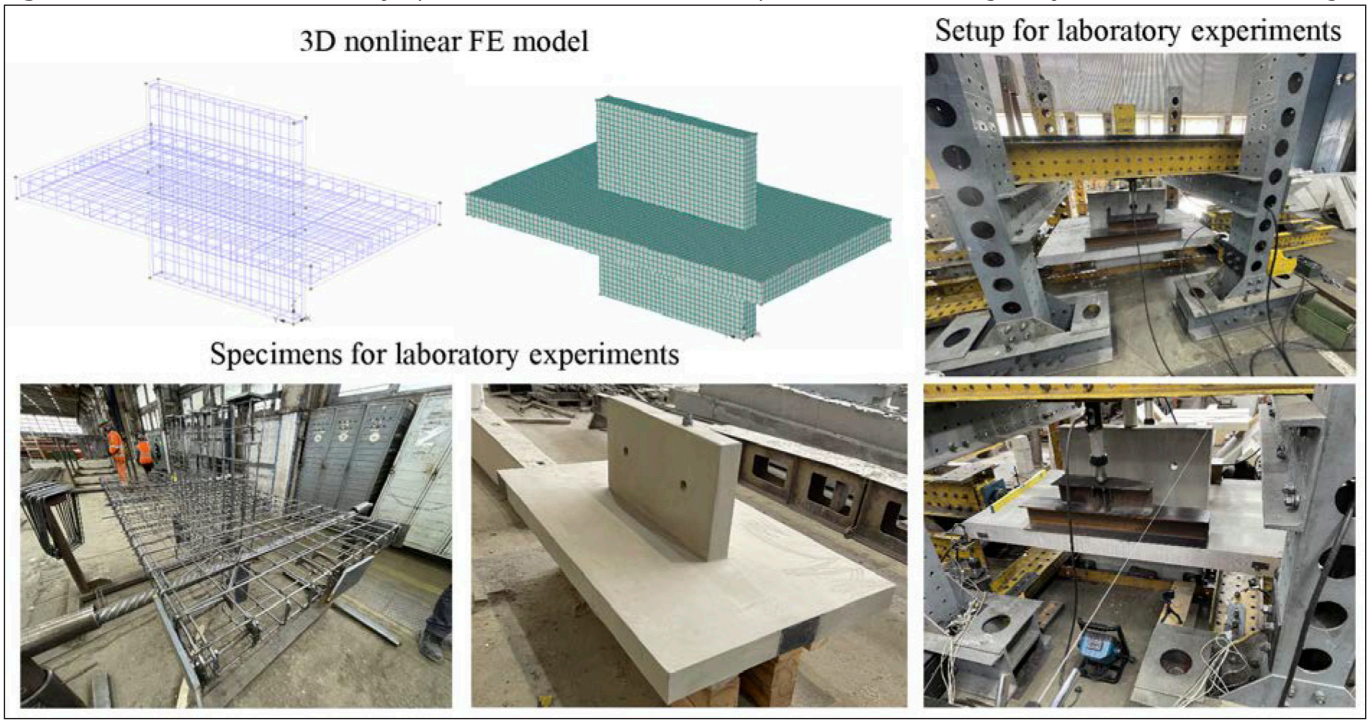

the literature. In our quasi-static studies, the results of the numerical models (cracking force, force of failure, peak force, displacement due to failure) showed only a difference of 5-10%. We also compared the crack patterns, which also showed a good agreement. Using the results and experiences obtained during our quasi-static studies, we also performed cyclic analyses, for which we also obtained very similar results (maximum difference: 10 %) within a certain rotation limit compared to the laboratory experiments. The results obtained during the cyclic studies can be extended to the case of larger deformations, which can be done by supplementing a modeling procedure. Based on the experience gained in the field of modeling of cast-in-situ reinforced concrete structures, we also extended the modeling procedure to the examination of prefabricated structural elements. Based on the study, it can be concluded that the joints and global behaviour of a simple prefabricated reinforced skeleton can be investigated with the modeling procedure developed and further developed by us. In any case, we need to compare the results with the results obtained in laboratory experiments to make sure that the modeling procedure is appropriate.

## 5. FURTHER RESEARCH OPPORTUNITIES

The results obtained and the modeling methods developed have laid the foundation for many studies by the research group we lead. Additional research areas as well as studies of structural designs have become available. Further developing the technique developed for the examination of basically cast-in-situ reinforced concrete structures, we are currently conducting research on prefabricated reinforced concrete structural elements and their connection design. The normal reinforced elements were started to be examined in respect of the foundation (column-cup neck) and column-beam relationship of a simple precast reinforced concrete skeleton. The modeling procedure available is elevated to a more advanced level by examining the prestressed structural elements of the prefabricated reinforced concrete and their connection design. Current research is underway on prefabricated prestressed reinforced concrete beams and prefabricated prestressed hollow core slabs. It should also be noted that the modeling procedure developed is also used in the numerical analysis of masonry structural element(s).

## 6. REFERENCES


Arjamadi S A., Yousefi M., Numerical Modeling of Seismic Behavior of Retrofitted RC Beam-Column Joints, *Civil Engineering Journal*, Vol. 4, No. 7, July 2018.

Červenka V., (1985). Constitutive Model for Cracked Reinforced Concrete. *ACI Journal*,*82*(6), 877-882.

Červenka, V., Jendele, L. and Červenka, J. (2014). ATENA Program Documentation Part 1, Theory *Červenka Consulting* s.r.o, 19.

Darwin, D., Pecknold, D.A.W., (1974). Inelastic Model for Cyclic Biaxial Loading of Reinforced Concrete, *Civil Engineering Studies*, University of Illinois, July.

***fib*** Model Code for Concrete Structures, 2010, *Wilhelm Ernst & Sohn,* Berlin, 2013

Haris I, Roszevák Zs., Előregyártott vasbeton gerendák numerikus és kísérleti vizsgálata, *Vasbetonépítés: A FIB magyar tagozat lapja: Műszaki folyóirat XIX*: (1) pp. 2-11., 2017.

Hawileh, R.A., Rahman, A., Tabatabai, H., (2010). Nonlinear finite element analysis and modeling of a precast hybrid beam-column connection subjected to cyclic loads. *Applied Mathematical Modelling*, *34*(9), 2562-2583.

Hordijk, D.A. (1991). Local Approach to Fatigue of Concrete, *Doctor dissertation*, Delft University of Technology, The Netherlands, ISBN 90/9004519-8.

Hwang, S-J., Lee, H-J., Analytical Model for Predicting Shear Strength of Exterior Reinforced Concrete Beam-Column Joints for Seismic Resistance, *ACI Journal*, V. 96, No. 5, September-October 1999.

Kolmar, W., (1986). Beschreibung der Kraftuebertragung über Risse in nichtlinearen Finite-Element-Berechnungen von Stahlbetontragwerken. *Dissertation*, T.H. Darmstadt, p. 94.

Kupfer, H., Hilsdorf, H.K., Rüsch, H. (1969). Behavior of Concrete under Biaxial Stress, *ACI Journal*, *66*(8), 656-666.

Masi A., Santeriero G., Nigro D., Cyclic Tests on External RC Beam-Column Joints: Role of Seismic Design Level and Axial Load Value on the Ultimate Capacity, *Journal of Earthquake Engineering*, 17:110–136, 2013.

Morgan J. (2000), „Structural Behavior in Concrete Frame Corners of Civil Defense Shelters, Thesis for the degree of doctor of philosophy", *Division of Concrete Structures, Department of Structural Engineering*, *Chalmers University of Technology*, Göteborg, Sweden

Roszevák Zs., Haris I. (2017). Comparison of different models on different cast-in-situ RC joints, *12th Central European Congress on Concrete Engineering 2017 Tokaj*, pp. 648-658.

Roszevák Zs., Bodó P. B., Haris, I., Vasbeton síklemez egyenértékű kerettel történő helyettesítése vízszintes teherre numerikus vizsgálatok alapján, *XIII. Magyar Mechanikai Konferencia*, Miskolc, 2019.

Roszevák Zs., Haris I., Monolit vasbeton keretsarok és oszlop gerenda kapcsolatok numerikus és kísérleti vizsgálata, *XIII. Magyar Mechanikai Konferencia*, Miskolc, 2019.

Roszevák Zs., Haris I. (2019), „Monolit vasbeton keretsarok numerikus vizsgálata - 1. rész Egyirányú monoton növekvő terhelés" *Vasbetonépítés: A FIB magyar tagozat lapja: Műszaki folyóirat XXI*: (3) pp. 78-86., 2019. doi/org/*10.32969/VB.2019.3.3*

Roszevák Zs., Haris I. (2020), „Monolit vasbeton keretsarok numerikus vizsgálata - 2. rész Ciklikusan változó terhelés" *VASBETONÉPÍTÉS: A **fib** magyar tagozat lapja: Műszaki folyóirat XXII*: (3) pp. 74-82., 2020. doi.org/10.32969/VB.2020.3.2

Roszevák Zs., Haris I. (2019). Finite element analysis of cast-in-situ RC frame corner joints under quasi static and cyclic loading, *Revista de la Construccion, 18*(3), 579-594.

Roszevák Zs., Haris I., (2021). The effect of non-linear finite element analysis on the description of the global behaviour of a prefabricated RC skeleton, *International Journal Optimization in Civil Engineering, 11*(3):515-546.

Santeriero G., Masi A., Finite Element Analysis of Experimental RC Wide Beam-Column Joints Provided with Different Detailing Solutions, COMPDYN 2017, *6th ECCOMAS Thematic Conference on Computational Methods in Structural Dynamics and Earthquake Engineering*, M. Papadrakakis, M. Fragiakadis (eds.), Rhodes Island, Greece, 15-17 June 2017.

Szczecina M., Winnicki A., (2015), „Numerical simulations of corners in RC frames using strut-and-tie method and CDP model", *XIII International Conference on Computational Plasticity, Fundamentals and Applications* COMLPAS XIII.

Yap, S. L., Li, B., (2011), „Experimental investigation of reinforced concrete exterior beam-column sub assemblages for progressive collapse" *ACI Structural, 108*(5), 542-552.

Van Mier, J.G.M., (1986). Multi-axial Strain-softening of Concrete, Part I: fracture, *Materials and Structures, RILEM*, 19(111).

Vecchio, F.J., Collins, M.P. (1986). Modified Compression-Field Theory for Reinforced Concrete Beams Subjected to Shear, *ACI Journal*, *83*(2), 219-231.



**Zsolt Roszevák** (1991) structural engineer MSc. (2016), research fellow at the Department of Structural Engineering, Budapest University of Technologies and Economics (Műegyetem rkp 3. H-1111, Hungary). Main field of interest: Experimental and numerical investigation of wall-slab type monolithic reinforced concrete connections. Member of the Hungarian Group of *fib* and the Hungarian Chamber of Engineers. roszevak.zsolt@emk.bme.hu

**István Haris, Ph.D.** (1980), structural engineer (2004), PhD (2013), associate professor at the Department of Structural Engineering, Budapest University of Technologies and Economics (Műegyetem rkp 3. H-1111, Hungary). Main field of interest: earthquake behaviour of masonry and reinforced concrete reinforcement elements. Member of the Hungarian Group of *fib* and the Hungarian Chamber of Engineers. haris.istvan@emk.bme.hu

# THE EFFECT OF SUPPLEMENTARY CEMENTITIOUS MATERIALS ON TRANSPORT PROPERTIES OF CEMENTITIOUS MATERIALS - STATE-OF-THE-ART


Zaid Ali Abdulhussein – Katalin Kopecskó

https://doi.org/10.32970/CS.2021.1.4

*The supplementary cementitious materials (SCMs) have recognized many of the beneficial influences on concrete ability to resist the penetration of chloride ions, such as fly ash, slag, silica fume, metakaolin, and other natural pozzolans; this benefit has primarily been ascribed to the refined pore structure that results from the appropriate use of SCMs, which, in turn, results in reduced permeability and ionic diffusivity. The paper illustrates the state-of-the-art research findings on; (1) the classification of the SCMs and physico-chemical properties; (2) the influences of SCMs on cement binder and the pore structure under chloride ion permeability; (3) the influences of the SCMs on the carbonation process of the cement binder that aims to determine the optimum relationship between SCMs and concrete transport properties. The interesting experimental investigations of the combined influence of chloride and carbonate permeation in cement binder that implement the latest methods in different curing conditions, types, and level contents of the SCMs will yield new scientific results and proposals for the industrial applications auxiliary materials.*

**Keywords:** supplementary cementitious materials, cement, transport properties, chloride migration, chloride diffusion, carbonation

## 1. INTRODUCTION

Supplementary cementitious materials (SCMs) are essential for producing high-performance concrete and preserving the environment (Ramezanianpour, 2014; Thomas, 2013). The main benefits of supplementary cementitious materials utilization in the cement and construction industry are threefold. First is the economic gain by replacing a substantial part of the Portland cement with cheaper natural pozzolans or industrial by-products. The second is lowering the blended cement environmental cost associated with the greenhouse gases emitted during Portland cement production. The third advantage is the durability improvement of the product. Additionally, even though the extensive blending of the SCMs with Portland cement is limited interference in conventional manufacturing, it provides the capability to take advantage, exploit of and immobilize considerable amounts of business and societal waste into construction substances (Snellings, 2012).

One of the most influencing factors on reinforced concrete structure's durability is the penetration of chloride ions to the steel reinforcement. De-icing roads with rock salt results in significant stress affected by the capillary pore system of concrete. Chlorides are well-known aggressive species for rebars of reinforced concrete (RC) structures. Therefore, the liquid water permeability and the chloride ion diffusion coefficient are involved as crucial parameters in governing equations of transport-related durability of concrete. Hence, it predicts the service life of RC structures. More precisely, the liquid water permeability is involved in the non-linear diffusion-type moisture transport equation (Baroghel-Bouny, 2007). Likewise, the apparent chloride ion diffusion coefficient is engaged in the non-linear diffusion-type equation of the penetration of chloride ions in concrete (Fick's second law) (Baroghel-Bouny, 2007). Thus, it ensures the theoretical relevance of these properties as regards the durability of RC structures.

## 2. SUPPLEMENTARY CEMENTITIOUS MATERIALS (SCMS) CLASSIFICATION

The general definition of supplementary cementitious material embraces many materials that vary widely in origin, chemical and mineralogical composition, and typical particle characteristics. However, it was generally accepted that the hydraulic or pozzolanic activity of SCMs depends primarily on their physicochemical properties rather than their origin (Snellings, 2012). On the one hand, two broad categories can be distinguished: (i) natural origin and (ii) materials of human-made or artificial origin. The former group consists of materials that can be used as SCM in their naturally occurring form. In most cases, they only need conditioning of particle characteristics by grinding and sieving processes. Typical natural SCMs are pyroclastic rocks, e.g., tuffs, either diagenetically altered or not, and highly siliceous sedimentary stones such as diatomaceous piles of earth. The group of artificial SCMs includes materials that have undergone structural modifications due to manufacturing or production processes. Artificial SCMs can be produced,

for instance, by thermal activation of kaolin-clays to obtain metakaolin; or can be obtained as waste or by-products from high-temperature processes such as blast furnace slags, fly ashes, or silica fume (Snellings, 2012).

## 2.1 Sources of SCMs

A wide variety of materials are available for use as SCMs, including raw and calcined natural minerals, biomass ashes, and industrial by-products. Some of these materials are described in Table 1, intended to showcase SCM resources' variety and availability (Snellings, 2016).

**Table 1:** *Materials used or considered as SCMs (Snellings, 2016)*

| Material | Chemistry composition | Used as SCM (Mt/y) | Total volume est. (Mt/y) | Comments |
|---|---|---|---|---|
| Blast furnace slag | Ca-Si-Al | 330 | 300–360 | Nearly fully used, latent hydraulic |
| Coal fly ash | Si-Al | 330–400 | 700–1100 | Subject to limitations on carbon content, reactivity |
| Natural pozzolans | Si-Al | 75 | Large accessible reserves | Large variety/variability, often high water demand |
| Silica fume | Si | 0.5–1 | 1–2.5 | Used in high-performance concrete |
| Calcined clays | Si-Al | 3 | Large accessible reserves | Metakaolin performs best, often high-water demand |

## 2.2 The Major Functions of SCMs Mechanisms

The result of the impact of SCMs is ruled via physics, chemistry, and thermodynamics. Dodson described that the effect of the SCMs on the properties of cement-based materials (Dodson, 2013) through:

- occur a reaction with the secondary product of cement hydration
- modify the kinetics of the hydration of cement in the mixture
- disperse cement particles in the mixture
- fill the pore spaces in cement paste.

## 2.3 Physical Properties and Chemical Compositions of the SCMs

The most widely used binder in concrete is the Ordinary Portland Cement (OPC), and the most effective SCMs used are fly ash, slag, silica fume, and metakaolin. Generally, the reactive components in SCMs are glassy or amorphous phases, and their intrinsic reactivity is determined primarily by the chemical composition and structure of these components. The main reactive phases for fly ashes and slags are aluminosilicate or calcium aluminosilicate glasses, respectively, with minor fractions of MgO, $Na_2O$, $K_2O$, and $Fe_2O_3$ incorporated (Lothenbach, 2011).

The primary characteristics measured in powder-type materials are specific surface area, particle size distribution, particle shape, and density from physical properties perspective. The specific surface area (defined on a mass basis) is the most common property used to describe Portland cement's fineness (Stark and Mueller, 2003). This surface area is an integral parameter that is of importance in defining concrete performance. The description of particle shape encompasses information about the angularity and sphericity, which affect workability and the physical phenomena utilized for particle size measurement (Naito, 1998). Tables 2 and 3, respectively, summarize the physical properties and chemical composition of common SCMs and OPC based on peer-reviewed publications (Panesar and Zhang, 2020; Sakir, 2020).

**Table 2:** *Physical properties of cement replacing materials (Panesar and Zhang, 2020)*

| Characteristics | Low-calcium FA | High-calcium FA | GGBS | SF | MK |
|---|---|---|---|---|---|
| Shape | Spherical | Spherical | Angular | Spherical | Angular, platy |
| Mean size (mm) | 5.0–73.5 | 2.0–73.5 | 13.8–22.2 | 0.1–0.3 | 1.0–20.0 |
| Surface area ($m^2$/kg) | 300–500 | 300–500 | 350–650 | 13,000–30,000 | - |

FA = Fly Ash; GGBS = Ground Granulated Blast-Furnace Slag; MK = Metakaolin; SF = Silica Fume

**Table 3:** *The chemical compositions of ordinary Portland cement (OPC) and different SCMs (Sakir, 2020)*

| CC (wt.%) | FA | SF | GGBS | MK | OPC |
|---|---|---|---|---|---|
| $SiO_2$ | 36–65 | 85–99 | 28–41 | 49–69 | 16–23 |
| CaO | 1–19 | 0–4 | 37–50 | 0–2 | 49–69 |
| $Al_2O_3$ | 17–29 | 0–6 | 5–14 | 25–44 | 4–7 |
| $Fe_2O_3$ | 4–31 | 0–3 | 0–1 | 0–3 | 2–7 |
| MgO | 0–7 | 0–5 | 4–10 | 0–3 | 0–5 |
| $SO_3$ | 0–3 | 0–2 | 0–3 | 0–1 | 0–1 |
| $Na_2O$ | 0–2 | 0–2 | 0–3 | 0–1 | 0–1 |
| $K_2O$ | 0–3 | 0–2 | 0–2 | 0–2 | 0–1 |
| $P_2O_5$ | 0–2 | 0–1 | – | 0–1 | – |
| LOI | 0–5 | 0–6 | 1–2 | 0–4 | – |
| Sp. gravity | 2.26 | 2.24 | 2.88 | 2.51 | 3.15 |

CC (wt.%) = Chemical Composition weight percentage; FA = Fly Ash; SF = Silica Fume; GGBS = Ground Granulated Blast-Furnace Slag; MK = Metakaolin; OPC = Ordinary Portland Cement.

# 3. RECENT REGULATIONS AND CODES FOR SCMS USED IN CONCRETE TECHNOLOGY

Figure 1 presents the relative compositions of Portland cement, fly ash, slag cement, silica fume, and metakaolin on a ternary phase diagram ($CaO–SiO_2–Al_2O_3$); and Table 4 presents the maximum allowable usage of each cement replacing material according to international standards (Panesar and Zhang, 2020).

The maximum specified allowable percentages of cement replacing materials in the standards are based on the activity

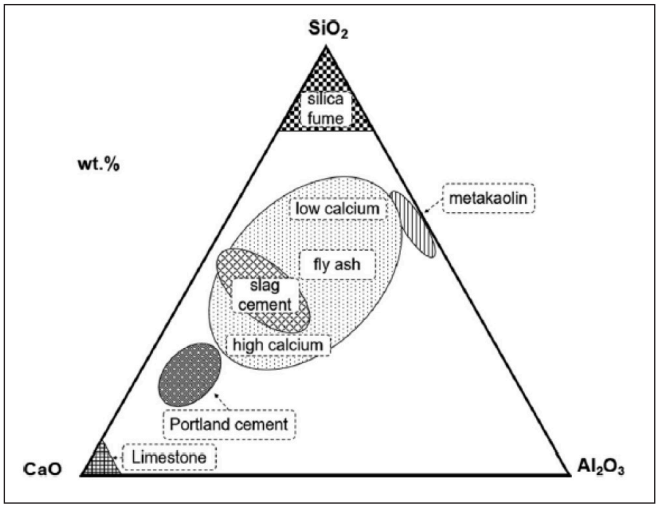


**Fig. 1:** *Ternary diagram supplementary cementing materials' composition (Panesar and Zhang, 2020)*

index of the utilized materials. The activity index can be measured by standardized methods; however, the impact of SCMs on cement hydration needs to be understood (Skibsted and Snellings, 2019).

**Table 4:** *Maximum specified allowable percentage of cement replacing materials based on national standards (contents in brackets indicate the cement type in each standard) (Panesar and Zhang, 2020)*

| SCMs | CSA A3000 (Canada) | ASTM C595; ASTM C150 (United States) | EN-197 BS-EN-197 (Europe and UK) | GB 175 (China) |
|---|---|---|---|---|
| GGBS | 70% | 95% | 95% (CEM III/C) | 20% (P.O)<br>50% (P.S.A)<br>70% (P.S.B) |
| Low/ high-Ca FA | 50% | 40% | 35% (CEM II/B-W)<br>35% (CEM II/B-V) | 20% (P.O)<br>20% (P.S.A)<br>40% (P.F) |
| MK | 40% | 40% | 35% (CEM II/B-Q) | Not specified |
| SF | 15% | - | 10% (CEM II/A-D) | Not specified |

GGBS = Ground Granulated Blast-Furnace Slag; FA = Fly Ash; MK = Metakaolin; SF = Silica Fume; P.O= Ordinary Portland Cement; (P.S.A and P.S.B= Portland Slag Cement (A and B type)); P.F= Portland Fly ash Cement.

# 4. TRANSPORT PROPERTIES OF THE CEMENTITIOUS MATERIALS

The ingress rate of deleterious species (e.g., water, chlorides, sulfates) from the service environment into the cement-based structures and components throughout their service life is defined as the material's transport properties. They are intrinsic durability properties to be considered at the materials research and structural design stages (Han, 2013). Therefore, pore structure, tortuosity, and permeability are considered vital properties of porous materials such as cement pastes, mortar or concrete, to understand their long-term durability performance. The chloride ion diffusion coefficient is considered a significant key parameter in governing equations of transport-related durability of concrete. As follows, a brief definition for this crucial parameter is given.

## 4.1 Chloride Diffusion Coefficients

Ollivier's study explains that two coefficients can be regarded as relevant durability indicators: (i) the effective chloride diffusion coefficient that appears in Fick's first law, and (ii) the apparent chloride diffusion coefficient can be derived from Fick's second law (Ollivier et al., 1998). The apparent chloride diffusion coefficients will be addressed, which can be regarded as more relevant for the (realistic) description of chloride ingress into concrete. This parameter also appears as a key parameter but may be more specific to the evaluation and prediction of RC structure's durability, hence the service life, concerning the risk of chloride-induced reinforcement corrosion. It is indeed Fick's second law, which is generally used to describe and predict the penetration of chlorides by "pure" diffusion in saturated concrete in non-steady-state (NSS) conditions (Baroghel-Bouny et al., 2007).

## 4.2 Influence of SCMs on Chloride Ion Permeability

Concrete permeability depends on multiple variables, such as combining composition quantities, compaction and curing, microcracks, and humidity conditions. The compressive strength and permeability of concrete are primarily influenced by capillary pores (El Mir et al., 2017; von Greve-Dierfeld et al., 2020). Based on the literature, with adequate curing, ground granulated blast furnace slag (GGBS), fly ash, and natural pozzolans generally reduce concrete permeability and absorption. The critical effect of SCMs, such as GGBS, on the concrete pore system is that large pores are minimized by blocking them with hydration products. The transform of continuous pores into discontinuous pores profoundly impacts concrete permeability (Kosmatka, Kerkhoff and Panarese, 2002). GGBS modifies the pore sizes and significantly decreases concrete permeability due to GGBS's reaction with calcium hydroxide and alkalis released during Portland cement hydration (Özbay, 2016). GGBS content a high level of aluminate, which is most likely responsible for the good binding characteristics. Additionally, the GGBS makes the cement matrix denser and diminishes the pore size. The ability of GGBS to protect against chloride-induced corrosion is attributed to the effective binding of free chloride ions (Kayali, 2012). Researchers showed that GGBS containing pastes have a higher chloride binding capacity than the PC control paste, which enhances C-S-H gel formation in concrete, hence providing larger surface areas available for adsorption (Kopecskó, 2006; Kopecskó and Balázs, 2017; Yuksel, 2018).

In a study presented by Güneyisi and Gesoğlu, it reported that the decrease of the chloride ions permeability of GGBS-containing concrete was due to changes in the pore structure of the hydrated cement system (Güneyisi and Gesoğlu, 2008). Gesoğlu et al. investigated the chloride ion permeability and water permeability of concretes containing GGBS from 0% to 60% substitution ratio with a 20% increment rate. They pointed out that the highest total charge passed in OPC concrete is controlled and can be defined as medium chloride

ion permeability concrete; the chloride ion permeability was decreased by 20%, 40%, and 60% GGBS substitution of OPC inconcretes. However, with the use of mineral additives, chloride ions passed became less (Gesoğlu, Güneyisi and Özbay, 2009). Therefore, GGBS improves the chloride resistivity of concrete made with the same water to cement ratio. A research study was investigated the chloride resistivity of concrete by performing a rapid chloride migration test (CTH-test; Tang and Nilsson, 1992). The result indicated that when the slag content of cement type is higher and the water to cement ratio remains constant, chloride penetration depths decrease. Concretes made with air-entraining agents and the same water to cement ratio, the chloride concertation at the same depth in the concrete increased; thereby the air-entraining agent increases the non-steady-state migration coefficient ($D_{nssm}$). This chloride resistivity reduction is due to the increased porosity, which causes permeability to increase. Eventually, it can conclude that the chloride migration coefficient and penetration depth decrease by increasing slag content considering the same ratio of water to cement. The experimental results indicated the lowest chloride migration coefficient, hence the highest chloride resistivity for concrete samples made with cement CEM III/B 32,5 N among the tested cements (Kopecskó and Balázs, 2017).

Aghaeipour and Madhkhan investigated the effect of GGBS on reinforced cement concrete (RCC) durability; for a minimum permeability, they suggested a 40% substitution ratio of OPC, as the durability characteristics such as water absorption, permeability, and freeze-thaw cycles were considered (Aghaeipour and Madhkhan, 2017).

Silica fume (SF) and calcined clay such as metakaolin (MK) are especially effective in this regard. They can provide concrete with a chloride resistance of under 1000 coulombs using the ASTM C 1202 rapid chloride permeability test (Barger, 1997). Experimental investigations show that as the quantity of hydrated cementing materials increases, the permeability of concrete decreases, and the water to cementitious materials (w/b) ratio decreases.

Recently the sulfate resistant Portland cement (SRPC), high-ferrite Portland cement (HFPC) application in ultra-high-performance concrete (UHPC) and self-compacting concrete (SCC) have been widely attractive, and it was expected to be used in the marine environment. Although, the main issue is the low chloride resistance. Thus, the effect of SCMs on chloride migration in HFPC precast concrete was carried out briefly in a recent report. The study reported that two SCMs, silica fume (SF) and metakaolin (MK), can significantly improve the steam cured HFPC concrete resistance to chloride permeation. The SF enhanced mechanism is based on optimizing the pore structure to retard chloride migration, while the role of MK is based on promoting the chloride binding capacity. This research could provide insight into a new precast concrete configuration with excellent resistance to sulfate and chloride in the marine environment (Huang et al., 2019). Additionally, the combined effect of MK and SF is beneficial rather than MK alone in improving the durability properties of ultra-high-performance concrete (UHPC) (El Mir et al., 2017). In the case of the SCC mixture, silica fume was noticed to have afast pozzolanic activity at an early age in comparison to metakaolin that has proved to possess a long-term effect on the improvement of chloride migration resistance. Furthermore, it observed at the highest bindery content (440 kg/m$^3$) that SF tended to be more effective in resistance chloride migration between than MK at similar

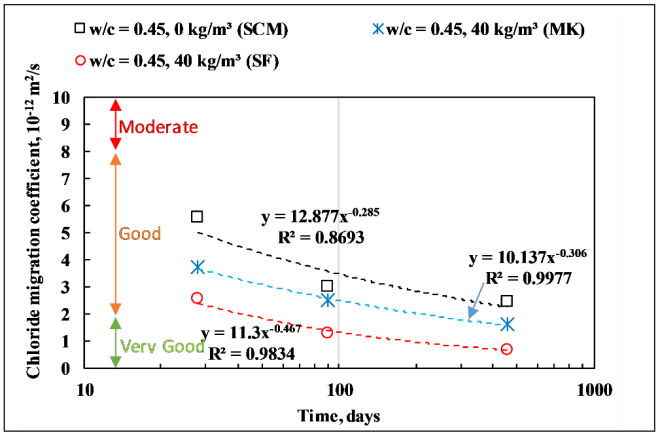


**Fig.2:** RCM for SCC mixtures incorporating MK at different levels of w/c as at 28, 90, and 460d (Courtesy of the author; El Mir, 2017).

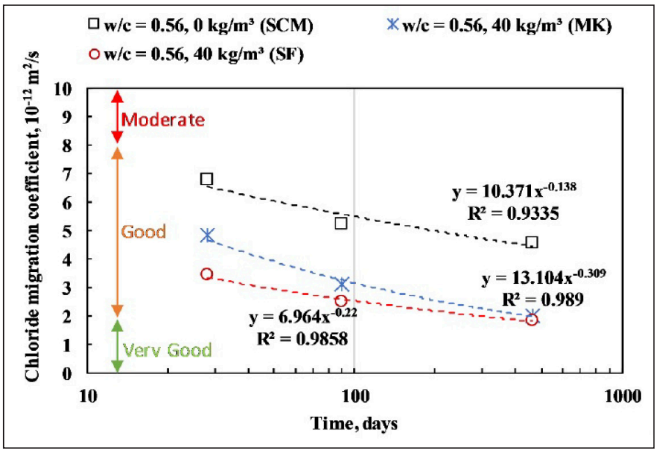


**Fig.3:** RCM for SCC mixtures incorporating MK at different levels of w/c as at 28, 90, and 460d (Courtesy of the author; El Mir, 2017).

percentages of mass replacement of cement; hence, SF is more effective in resistance chloride migration between 10-12.5% of mass replacement of cement, hence with the time progress, the further improvement on the chloride migration resistance of SCC containing SF is rather slight as compared to metakaolin at 460 days as shown in Figures 2 and 3 (El Mir, 2017).

## 5. CARBONATION REACTION

Concrete structures with reinforcing steel often face serious durability problems in the material's service that deteriorate with age progressively. The long-term ingress of environmental substances, such as seawater, marine aerosol, carbon dioxide ($CO_2$), and sulfate; caused primarily the material's deterioration in the reinforced concrete structure. Among the aggressive substances, the $CO_2$ from the atmosphere can diffuse through the concrete pore structure, dissolving in the pore solution and reacting with the hydrated calcium compounds (Hussain, Bhunia, and Singh, 2017). This physicochemical phenomenon in cementitious materials is known as carbonation. The carbonation reaction takes place in cementitious materials with the governing reactions shown by Eqs. (1) and (2) (Papadakis, Vayenas and Fardis, 1991):

$$Ca(OH)_2 + CO_2 \rightarrow CaCO_3 + H_2O \quad (1)$$

$$xCaO \cdot ySiO_2 \cdot zH_2O + xCO_2 \rightarrow xCaCO_3 + y(SiO_2 \cdot tH_2O) + (z\text{-}yt)H_2O \quad (2)$$

$Ca(OH)_2$ and C-S-H are the two primary hydration

compounds susceptible to $CO_2$ in cementitious materials. The carbonation causes a reduction in the alkalinity of pore solution for concrete cover, which is thought of as a chemical degradation towards the RC structure with steel bars (Stefanoni, 2018). The development of a passive film of ferrous oxide at the surface of steel reinforcement that prevents the steel from aggressive corrosion requires a strongly alkaline environment within concrete (Zhang, 2017). When the carbonation front propagates, the alkalinity of the pore solution reduces. Thus, the initially formed passive film is gradually destroyed, and consequently, the time of initiating steel corrosion can be sharply shortened in RC structures. Additionally, the corrosion risk of steel reinforcement increases with exposure to moisture, oxygen, and even chloride ions; hence, steel corrosion induces rust expansion stress on the surrounding concrete, causing cracks in the concrete cover. This cracking situation further promotes the penetration of $CO_2$ and other aggressive ions from the environment, which exacerbates RC structure's deterioration in the construction field. In addition to reducing alkalinity, carbonation significantly reduces the chloride binding capacity and increases the chloride ion diffusion rate in concrete (Zhang, 2017; Liu, 2017).

## 5.1 Influence of the SCMs on the Carbonation

Through the carbonation, a relatively high amount of calcium silicate hydrate (C-S-H) with a low Ca/Si ratio will carbonate in cement paste blended with SCMs. According to a study implemented by Schubert, pointed out that the action of SCMs is twofold since they are associated with the consumption of $Ca(OH)_2$ in the pozzolanic reaction, which reduces the pH and increases the rate of carbonation, while at the same time the formation of new C-S-H blocks capillary pores and decreasing carbonation (Schubert, 1987). Park found that the greater the amount of pozzolanic materials, the deeper the carbonation depth becomes (Park, 1995). A researcher stated that this phenomenon is primarily due to reducing the alkali content in cementitious materials. The calcium silicate hydrate formed from the pozzolanic reaction absorbs more alkali ions, hence, lowering the concrete's pH level (Mindess, Young and Darwin, 2003). A study has been conducted to determine the pore volume and size distribution of capillary pores using a Mercury Intrusion Porosimeter (MIP). Results reveal that carbonation of most of the species of C-S-H results in increasing porosity of cement paste. The total and effective capillary porosity of pastes blended with a high amount of GGBS increased after carbonation (Wu and Ye, 2017). Vineet has been investigated the carbonation resistance of cement that containing (SCMs) under the exposition of the carbon dioxide concentrations of 1% and 3%, relative humidity of 40%, 60%, and 80%, and temperature of 27 ℃ and 45 ℃ at two different water to binder ratio. The investigation reveals that the carbonation rate is dictated mainly by the degree of replacement of the clinker. Relatively to the percentage of water to binder and humidity, concrete made with cement-slag blends reveals more significant carbonation than mixtures containing other SCMs (Shah and Bishnoi, 2018). A study conducted by Bouikni mentions that concrete with 65% slag replacement always showed higher carbonation penetration than concrete with 50% slag and that water curing is a significant factor in reducing carbonation (Bouikni, 2009).

An investigation of the influence of silica fume (SF) on the carbonation depth, reporting that higher carbonation depths are associated with the use of SF, some studies confirmed these results (Skjolsvold, 1986; Grimaldi, Carpio and Raharinaivo, 1989; Khan and Lynsdale, 2002). A researcher studied several SCMs (SF, low- and high-calcium fly-ash), noting that the carbonation depth decreases as the aggregate replacement by SCMs increases, the carbonation depth increases as cement replacement by SCMs increases (Papadakis, 2000). Kulakowski and Lewis mentioned an increase in concrete carbonation when fly-ash (FA) is used (Ho and Lewis, 1983). Gonen and Yazicioglu indicated that the depth of the carbonation of reference concrete mixes was slightly lower than that containing FA. Simultaneously, in concrete mixtures containing silica fume and fly-ash (SFAC), the carbonation depth was lower than that of other concrete mixes, where silica fume had little effect on carbonation. These authors attribute the lower depth of carbonation in SFAC to their lower porosity; they observe that the porosity of FA mixtures was double that of the SFAC concrete (Gonen and Yazicioglu, 2007).

Curing conditions has a significant influence on the carbonation depths in concrete mixtures. A study investigated in the case of fly-ash concrete mixes; the carbonation depths are about 20-50% higher in the case of air-curing than in the case of water-curing due to the diffusion of $CO_2$, which is affected by the water saturation degree in the mixture. Thus, the drier the porosity, the higher the $CO_2$ diffusion, and as a consequence, the faster and higher carbonation depth occur (Younsi, 2011). Bai has been studied the PC-PFA-MK concrete mixes, revealing two major trends: (i) increasing PC replacement with PFA raises the depth of carbonation, and (ii) systematically replacing PFA (pulverized fly ash) with increasing MK levels decreases the depth of carbonation. A strong correlation between reduced carbonation depth and reduced sorptivity was also recorded (Bai, 2002). The resistance of compound mixtures of PC-MK, PC-GGBS, and PC-GGBS-MK against the chloride ion penetration and carbonation depth, shows the mix proportion of 10% GGBS and 10% MK shows an evident influence on decreasing the chloride ion migration coefficient and carbonation depth; PC-MK was more effective than PC-GGBS. Among all the specimens, the compound mixture of GGBS and MK (PC-GGBS-MK) presented the most beneficial influence to improve the chloride penetration resistance and to enhance concrete carbonation resistance (Duan, 2013).

According to the summarized literature of the report that RILEM TC 281-CCC recently conducted, indicated that with the reduced portlandite content in SCM containing systems, rapidly the carbonation will happen in the main $CO_2$-binding phases, C-S-H in the case of using SF, and C-A-S-H phases in the case of using GGBS, FA, MK, and other Al-containing SCMs. It seems to be that the carbonation of these hydrates is a significant contributor to carbonation shrinkage (polymerization shrinkage), especially at low Ca/Si ratio C(-A)-S-H, and induces coarsening of pore structure upon carbonation and reduce the mechanical strength. Additionally, upon the carbonation, the porosity of cementitious materials increases with increasing SCMs replacements ratio (von Greve-Dierfeld et al., 2020).

## 5.2 Combined Effect of the Carbonation and SCMs on Chloride Permeability

The durability of concrete structures is a frequent significant investigating issue, and it considerably impacts the service life of the concrete structures. Since the actual structures are more likely to experience deterioration due to the combination of more than two factors rather than the action of a unique factor, researchers in advanced countries recently attempted actively to investigate the chloride ions penetration under the combined action of carbonation, freezing-thawing, and salt attack. The penetration depth of chloride ion and carbonation depth was investigated in an environment subjected simultaneously to salt attack and carbonation (Tumidajski and Chan, 1996). The most crucial degradation among the multiple deterioration processes could be seen to be the corrosion of reinforcement due to chloride ions penetration, especially in the case of nuclear power plant (NPP) structures located in a coastal area.

The impacts of chloride content on carbonation in concretes has frequently considered; in comparison, the investigations of the carbonation influence on the progress of chloride penetration is limited. With the utilization of the replacement of supplementary cementitious materials (SCMs), the results of the carbonation depth of GGBS and PFA samples are higher than of mixes without these materials by using phenolphthalein indicator and XRD analysis. The results of the depth of the carbonation for the mixtures incorporating SCMs (PFA and GGBS) have less $Ca(OH)_2$ than the OPC mixtures at a different depth. Hence, at a deep depth, the relative intensities of $Ca(OH)_2$ remain low, but the concentration of $CaCO_3$ stays high (Al-Ameeri, 2018). An investigated study points out the carbonation effect on the chloride penetration and replacing OPC by GGBS and PFA in cracked concrete samples. The depth of chloride ($DoCl^-$) and carbonation (DoC) was explored by using an accelerated environment test programmed ($CO_2$ and $Cl^-$). The depth of carbonation was determined by the phenolphthalein indicator, whereas the $DoCl^-$ was measured by $AgNO_3$ spraying. Two series of concrete samples were tested for chloride penetration. The series differences are that the first was exposed to an accelerated $CO_2$ environment, while the second was exposed to a typical $CO_2$ environment and exposure time to $CO_2$ for both was five weeks. Results for the two series for different crack widths and w/c ratios are presented in Tables 5 and 6.

**Table 5:** Chloride penetration depth ($DoCl^-$) mm for samples used in (series 1) (Al-Ameeri et al., 2021)

| Sample - w/c ratio | Un-cracked | Cracked width 0.1 mm | Cracked width 0.2 mm | Cracked width 0.3 mm | Cracked width 0.4 mm |
|---|---|---|---|---|---|
| M 0.4 | 24 | 30 | 30 | 29 | 35 |
| M 0.5 | 35 | ≥40 | ≥40 | ≥40 | ≥40 |
| M 0.6 | ≥40 | ≥40 | ≥40 | ≥40 | ≥40 |
| M 0.5 +GGBS | 15 | 25 | 29 | 30 | 33 |
| M 0.5 + PFA | 14 | 23 | 22 | 25 | 27 |

**Table 6:** Chloride penetration depth ($DoCl^-$) mm for samples used in (series 2) (Al-Ameeri et al., 2021)

| Sample - w/c ratio | Un-cracked | Cracked width 0.1 mm | Cracked width 0.2 mm | Cracked width 0.3 mm | Cracked width 0.4 mm |
|---|---|---|---|---|---|
| M 0.4 | 27 | 33 | 31 | 34 | 39 |
| M 0.5 | ≥40 | ≥40 | ≥40 | ≥40 | ≥40 |
| M 0.6 | ≥40 | ≥40 | ≥40 | ≥40 | ≥40 |
| M 0.5 +GGBS | 15 | 29 | 31 | 31 | 31 |
| M 0.5 + PFA | 20 | 25 | 26 | 27 | 30 |

The chloride ion penetration increases significantly within the concrete samples exposed to the $CO_2$ environment for all mixes used in the study. There is a significant decrease of chloride ions penetration in carbonated and uncarbonated concretes incorporating SCMs when compared to the reference concretes. Additionally, for concrete specimens exposed to carbonation and chlorides, crack widths affect the penetration of chloride and, therefore, must be taken into consideration in service life prediction models (Al-Ameeri et al., 2021).

Generally, the pozzolanic materials improve the durability of the concrete, especially for chloride penetration (Chindaprasirt, Rukzon and Sirivivatnanon, 2007), such as silica fume (SF), metakaolin (MK), ground palm oil fuel ash (POA), ground rice husk ash (RHA) and fly ash (FA). A study had been conducted on the influence of carbon dioxide on the chloride ion penetration and diffusion coefficient in OPC mortar containing partial replacement of (RHA, POA and FA) with constant water-cement ratio and under a testing environment with 5% of $CO_2$ and 30 days of immersion in 3% of NaCI solution. From the test, it can be concluded that in normal circumstances, the incorporation of pozzolans such as POA, RHA and FA are very beneficial to the performance of mortar in terms of chloride resistance. In terms of exposure to a high level of carbon dioxide concentration, the resistance to chloride penetration of mortar containing pozzolans is lowered and renders the mortar susceptible to chloride attack depending on the type and level of replacement. Eventually, mortars with RHA show the best performance in terms of chloride penetration resistance. FA and POA and the blend of these pozzolans produce mortars with reduced resistance to chloride penetration as a result of exposure to carbon dioxide (Chindaprasirt, 2008).

The corrosion of concrete structures has received significant attention related to the deterioration of sea-side structures, such as new airports, bridges, and nuclear power plants. In this regard, many studies have done on the chloride attack in concrete structures. However, an investigation study explored the influences of carbonation to chloride attack in concrete structures by utilizing fly ash as a partial cement substitute. The major test variables considered in this study are fly ash and w/c ratio to examine the chloride ion penetration effects in concrete for the case where the carbonation was exerting. Eventually, the investigation result showed that the admixing of fly ash is highly efficient in preventing the penetration of chloride ions under a single condition when carbonation is exerting combined action, the concentration of chloride ion tends to be high until an actual depth, but the concentration of

chloride ion decreases suddenly beyond a certain limit depth, which minimizes its effect on the corrosion of reinforcement according to the admixing of fly ash even under the combined action of the carbonation (Oh, Lee, Lee and Jung, 2003).

# 6. CONCLUSIONS

The article is an attempt to summarize the current state of the SCMs performance in cement composites and their advanced influences on chloride ion permeability and carbonation behaviour. Various influencing factors have been considered, including curing conditions, mixture proportion, temperatures and w/b ratio. Overall, the interesting experimental results would significantly contribute to developing a more systematic, comprehensive, and accurate mathematical model for describing the behaviour of the materials. Based on the literature research, the main conclusions are as follows:

- The supplementary cementitious materials, as SF, GGBS, and MK, show a significant impact on permeability and sorption characteristics of concrete, specifically on the pore structure of the concrete and chloride ion's binding capacity. The GGBS and MK have beneficial effects on promoting the effective binding capacity of free chloride ions, while the SF's enhancement mechanism is based on the optimization of the pore structure to retard the chloride ion migration.
- The carbonation system of cementitious materials containing SCMs is different from the Portland cement system due to the different pore structures and pore solution chemistry. The carbonation will happen rapidly by reducing the content of the non-consumed portlandite in the SCMs containing system.
- The porosity of concrete in terms of chloride ion permeability and carbonation resistance is sensitive to material factors, such as w/b ratio, curing type, humidity, and level of replacement of the clinker, which is directly influencing.
- The binary and ternary mixtures of SCMs show a beneficial improvement in the carbonation depth due to their lower porosity; it shows a correlation between reduced carbonation and reduced sorptivity, the concrete's carbonation resistance improving with substantial and sufficient curing periods.
- Among the most effective common SCMs, metakaolin (MK) shows a beneficial effect on the concrete's durability. It improves the resistance against chloride penetration (decreases the chloride ion permeability) by enhancing the chloride ion binding capacity and also reduces the carbonation depth of concrete in the case of mono (one kind of SCMs used as cement substitution in mixture), binary and ternary mixes.
- Pozzolanic materials improve the durability of the concrete, especially for chloride penetration; in the case of the combined effects of carbonation on chloride penetration resistance in concrete, the levels and types of SCMs replacement effects the ability of concrete to resist the penetration of chloride ions. Therefore, the crack widths affect the penetration of chloride, hence, must be taken into consideration in service life prediction models.
- The high level of the SCMs replacement in concrete may show a lower effect on the carbonation resistance due to their consumption of $Ca(OH)_2$ in pozzolanic reaction, which reduces the pH level in concrete, consequently, increase the carbonation depth and reduce the ability of these materials to resist other forms of deterioration, determination of the influence of high SCMs on carbonation resistance; long-term experiments are needed, respectively.

# ACKNOWLEDGEMENTS

The scholarship support provided for the PhD study and research work to the first author by *Stipendium Hungaricum* Scholarship Program is gratefully acknowledged.

The authors acknowledge the support by the Hungarian Research Grant NVKP_16-1-2016-0019 "Development of Concrete Products with Improved Resistance to Chemical Corrosion, Fire or Freeze-Thaw".

# 7. REFERENCES

Aghaeipour, A. and Madhkhan, M. (2017), "Effect of ground granulated blast furnace slag (GGBS) on RCCP durability," *Construction and Building Materials*, vol. 141, pp. 533-541.

AL-Ameeri, AS, Nahhab, AH, AL-Baghdadi, HM. (2021 ), "the effects of carbonation on the chloride resistance of concretes with supplementary cementitious materials (SCMs) ". *In Young Researchers' Forum V* (p. 5).

Al-Ameeri, A., Rafiq, M., & Tsioulou, O. (2018), ". Influence of cracks on the carbonation resistance of concrete structures". *In Sixth International Conference on the Durability of Concrete Structures*, University of Leeds (pp. 358-367)

ASTM, C. (2002). 150, Standard specification for Portland cement. *Annual book of ASTM standards*, 4, 134-138.

ASTM, C. (2003). 595. Standard Specification for Blended Hydraulic Cements. *Annual book of ASTM standards*, 4.

ASTM C1202, 2000, "Electrical indication of concrete's ability to resist chloride ion penetration", *Annual Book of American Society for Testing Materials Standards*, vol. C04.02,.

Bai, J., Wild, S. and Sabir, B.B. (2002), "Sorptivity and strength of air-cured and water-cured PC–PFA–MK concrete and the influence of binder composition on carbonation depth," *Cement and Concrete Research*, vol. 32, no. 11, pp. 1813-1821.

Barger, G.S., Lukkarila, M.R. and Martin, D.L. (1997), "Evaluation of a blended cement and a mineral admixture containing calcined clay natural pozzolans for high performance concrete", *in International Purdue Conference on Concrete Pavement Design and Materials for High Performance*, 6th, 1997, Indianapolis, Indiana, U.S.A. vol. 1. pp,131-47.

Baroghel-Bouny, V. Thiery, M. and Barberon, F. (2007), "Assessment of transport properties of cementitious materials: a major challenge as regards durability" *Revue Européenne de génie civil*, vol. 11, no. 6, pp. 671-696.

Bouikni, A., Swamy, R N. and Bali, A. (2009), "Durability properties of concrete containing 50% and 65% slag," *Construction and Building Materials*, vol. 23, no. 8, pp. 2836-2845.

Canadian Standards Association. (2013). CSA A3000-13 Cementitious Materials Compendium. CSA Group, Mississauga, Ontario.

Chindaprasirt, P, Rukzon S and Sirivivatnanon, V. ( 2007), "Rresistance to chloride penetration of blended Portland cement mortar containing palm oil fuel ash, rice husk ash and fly ash" *Construction and Build Materials*, doi:10.1016/j.conbuildmat.2006.12.001.

Chindaprasirt, P, Rukzon, S, Sirivivatnanon, V. (2008), "Effect of carbon dioxide on chloride penetration and chloride ion diffusion coefficient of blended Portland cement mortar". *Construction and Building Materials*, Vol. 22, Issue 8, Pages 1701-1707, https://doi.org/10.1016/j.conbuildmat.2007.06.002.

Dodson, H. (2013), Concrete admixtures: *Springer Science & Business Media*.

Duan, P., Shui, Z., Chen, W. (2013), "Enhancing microstructure and durability of concrete from ground granulated blast furnace slag and metakaolin as cement replacement materials," *Journal of Materials Research and Technology*, vol. 2, no. 1, pp. 52-59.

El Mir, A.I. (2017). Influence of additives on the porosity related properties of self-compacting concrete. *PhD Thesis*. p109.

El Mir, A.I., Vági, I., Sinka, Z., & Nehme, S.G., (2017),."Properties of ultra high performance concrete made utilizing supplementary cementitious materials", *11th HPC and the Second Concrete Innovation Conference (2nd CIC)*, Tromsø, Norway, Vol. 978-82, no. 61, pp. 11.

EN, B.S., (2000). 197-1. Cement–Part 1: Composition, specifications and conformity criteria for common cements. *British Standards Institution*.

Gesoğlu, M., Güneyisi, E. and Özbay, E. (2009), "Properties of self-compacting concretes made with binary, ternary, and quaternary

cementitious blends of fly ash, blast furnace slag, and silica fume," *Construction and Building Materials*, vol. 23, no. 5, pp. 1847-1854.
Gonen, T. and Yazicioglu, S. (2007), "The influence of mineral admixtures on the short and long-term performance of concrete," *Building and Environment*, vol. 42, no. 8, pp. 3080-3085.
Grimaldi, G., Carpio, J. and Raharinaivo, A. (1989), "Effect of silica fume on carbonation and chloride penetration in mortars", *in Third CANMET/ ACI International Conference on Fly Ash, Silica Fume, Slag and Naural Pozzolans in Concrete*, pp. 320-334.
Güneyisi, E., Gesoğlu, M. (2008), "A study on durability properties of high-performance concretes incorporating high replacement levels of slag," *Construction and Building Materials,* vol. 41, no. 3, pp. 479-493.
Han, B., Yang, Z. and Shi, X. (2013), "Transport properties of carbon-nanotube/cement composites," *Journal of Materials Engineering and Performance*, vol. 22, no. 1, pp. 184-189.
Ho, DWS, and Lewis, R.K. (1983), "Carbonation of concrete incorporating fly ash or a chemical admixture," *Special Publication*, vol. 79, pp. 333-346.
Huang, X., Hu, S. and Wang, F. (2019), "The effect of supplementary cementitious materials on the permeability of chloride in steam cured high-ferrite Portland cement concrete," *Construction and Building Materials*, vol. 197, pp. 99-106.
Hussain, S., Bhunia, D., and Singh, S.B. (2017), "Comparative study of accelerated carbonation of plain cement and fly-ash concrete," *Journal of Building Engineering*, vol. 10, pp. 26-31.
Kayali, O., Khan, H., and Ahmed, S. (2012), "The role of hydrotalcite in chloride binding and corrosion protection in concretes with ground granulated blast furnace slag," *Cement and Concrete Composites,* vol. 34, no. 8, pp. 936-945.
Khan, M.I. and Lynsdale, C. J. (202), "Strength, permeability, and carbonation of high-performance concrete," *Cement and Concrete Research*, vol. 32, no. 1, pp. 123-131.
Kopecskó, K. "Chloride ion binding capacity of clinker minerals and cements influenced by steam curing (in Hungarian: *A gőzölés hatása a cement klinkerek és cementek kloridion megkötő képességére*)", PhD Thesis, 2006. p.100
Kopecskó, K., and Balázs, G.L. (2017), "Concrete with improved chloride binding and chloride resistivity by blended cements", *Advances in Materials Science and Engineering*, pp. 13, https://doi.org/10.1155/2017/7940247
Kosmatka, S.H., Kerkhoff, B. and Panarese, W.C., (2002), Design and control of concrete mixtures, *Portland Cement Association Skokie, IL*., (Vol. 5420, pp. 60077-1083).
Liu, J., Qiu, Q., Chen, X., Xing, F., Han, N., He, Y., and Ma, Y. (2017), "Understanding the interacted mechanism between carbonation and chloride aerosol attack in ordinary Portland cement concrete," *Cement and Concrete Research*, vol. 95, pp. 217-225.
Lothenbach, B. Scrivener, K. and Hooton, C. (2011), "Supplementary cementitious materials," *Cement and Concrete Research*, vol. 41, no. 12, pp. 1244-1256.
Mindess, S., Young, F.J., and Darwin, D. (2003), "Concrete 2nd Editio," Technical Documents.
Naito, M., Hayakawa, O. and Nakahira, K. (1998) "Effect of particle shape on the particle size distribution measured with commercial equipment," *Powder Technology*, vol. 100, no. 1, pp. 52-60.
Oh, B. H., Lee ,S. K., Lee, M. K, Jung, S. H. (2003), "Influence of carbonation on the chloride diffusion in concrete". *Journal of the Korea Concrete Institute*.; vo.15, no.6, pp.829-39.
Ollivier, J.P., Marchand, J., Nilsson, LO. ( 1998), "Methodology of chloride ion penetration prediction by diffusion in concrete (in French)", Proc. of Int. RILEM Conf. "*Concrete: From material to structure*", 11-12 September 1996, Arles, France (Ed. by J.P. Bournazel & Y. Malier, RILEM, Paris), p. 166-195
Özbay, E., Erdemir, M. and Durmuş, İ. (2016), «Utilization and efficiency of ground granulated blast furnace slag on concrete properties–A review," *Construction and Building Materials*, vol. 105, pp. 423-434.
Pacheco-Torgal, F., Miraldo, S. and Labrincha, J. (2012), "An overview on concrete carbonation in the context of eco-efficient", *Construction and Building Materials*, Vol. 36, , Pages 141-150, https://doi.org/10.1016/j.conbuildmat.2012.04.066
Panesar, K. and Zhang, C. (2020), "Performance comparison of cement replacing materials in concrete: Limestone fillers and supplementary cementing materials–A review" *Construction and Building Materials,* vol. 251, pp. 118866, 2020.
Papadakis, V.G. (2000), "Effect of supplementary cementing materials on concrete resistance against carbonation and chloride ingress," *Cement and concrete research*, vol. 30, no. 2, pp. 291-299.
Papadakis, V.G., Vayenas, C.G., and Fardis, M. N. (1991), "Experimental investigation and mathematical modeling of the concrete carbonation problem," *Chemical Engineering Science*, vol. 46, no. 5-6, pp. 1333-1338.
Park, G. K. (1995). Durability and carbonation of concrete. *Mag Korean Concr Inst*, 7, 74-81.
Ramezanianpour, A. (2014) "Cement replacement materials", *Springer Geochemistry/Mineralogy*, vol. 10, pp. 978-3.
Sakir, S., Raman, S.N. and Safiuddin, M. (2020), "Utilization of by-products and wastes as supplementary cementitious materials in structural mortar for sustainable construction", *Sustainability*, vol. 12, no. 9, pp. 3888.
Schubert, P. (1987), "Carbonation behavior of mortars and concretes made with fly ash" *Special Publication*, vol. 100, pp. 1945-1962.
Shah, V. and Bishnoi, S. (2018), "Carbonation resistance of cements containing supplementary cementitious materials and its relation to various parameters of concrete", *Construction and Building Materials*, vol. 178, pp. 219-232.
Skjolsvold, O. (1986), "Carbonation depths of concrete with and without condensed silica fume", *Special Publication*, vol. 91, pp. 1031-1048.
Snellings, R. Mertens, G. and Elsen, M. (2012) "Supplementary cementitious materials," *Reviews in Mineralogy and Geochemistry*, vol. 74, no. 1, pp. 211-278.
Snellings, R. (2016), "Assessing, understanding and unlocking supplementary cementitious materials" *RILEM Technical Letters*, vol. 1, pp. 50-55.
Standard, C. C. (2007). Common portland cement (GB175-2007). Beijing: *Chinese National Standard*.
Stark, U. and Mueller, A. (2003), "Particle size distribution of cements and mineral admixtures - standard and sophisticated measurements", *in 11th International Congress on the Chemistry of Cement (ICCC*), Durban.
Stefanoni, M., Angst, U., and Elsener, B. (2018), "Corrosion rate of carbon steel in carbonated concrete–A critical review", *Cement and Concrete Research*, vol. 103, pp. 35-48.
Tang, L. and Nilsson, L.O. (1992) "Chloride diffusivity in high strength concrete" *Nordic Concrete Research*, vol. 11, pp. 162–170.
Thomas, M. (2013), Supplementary cementing materials in concrete: *CRC press*.
Tumidajski, PJ and Chan, GW. (1996),"Effect of sulfate and carbon dioxide on chloride diffusivity", *Cement and Concrete Research*. 1;26(4):551-6.
von Greve-Dierfeld, S., Lothenbach, B. and Vollpracht, A. (2020), "Understanding the carbonation of concrete with supplementary cementitious materials: a critical review by RILEM TC 281-CCC", *Materials and Structures*, vol. 53, no. 6, pp. 1-34.
Wu, B. and Ye, G. (2017), "Development of porosity of cement paste blended with supplementary cementitious materials after carbonation", *Construction and Building Materials, vol*. 145, pp. 52-61.
Younsi, A., Turcry, P., Rozière, E., Aît-Mokhtar, A. and Loukili, A. (2011), "Performance-based design and carbonation of concrete with high fly ash content" *Cement and Concrete Composites*, vol. 33, no. 10, pp. 993-1000.
Yuksel, I. (2018), "Blast-furnace slag, Waste and Supplementary Cementitious Materials in Concrete", *Woodhead Publishing*, vol.: Elsevier, pp. 361-415.
Zhang, J., Ma, H., Pei, H. and Li, Z., (2017), Steel corrosion in magnesia–phosphate cement concrete beams", *Magazine of Concrete Research*, vol. 69, no. 1, pp. 35-45.

**Zaid Ali Abdulhussein:** PhD student in Civil Engineering in the Department of Construction Materials and Technologies at the Budapest University of Technology and Economics in Hungary (Supervisor: Katalin Kopecskó PhD). He graduated in Civil Engineering from the National University of Malaysia (2018). His main research fields are the durability of concrete and other materials, supplementary cementitious materials, transport properties of cementitious materials, and construction materials' deterioration processes. Email: zaid.abdulhussein695@edu.bme.hu

**Katalin Kopecskó:** Associate Professor at the Budapest University of Technology and Economics in Hungary. Graduated in Chemical Engineering (1990) and has postgraduate studies in Concrete Technology (2004). She has PhD degree since 2006. She teaches Chemistry for Civil Engineers (BSc), Material Science for Civil Engineers (MSc), and Alkali activated materials in Civil Engineering (PhD) subjects. Her research fields are deterioration processes of construction materials, the durability of concrete and other materials, cement hydration, diagnostics, mineralogical and microstructural analysis, X-ray diffraction (XRD), thermal analyses (TG/DTG/DTA), scanning electron microscopy (SEM). She is a member of the Hungarian Group of *fib* and the Technical Committee MSZT/MB 102 (Cement and Lime) in the Hungarian Standards Institution. Email: kopecsko.katalin@emk.bme.hu

# FERROBETON

A CRH COMPANY

**safe basis provided by concrete**

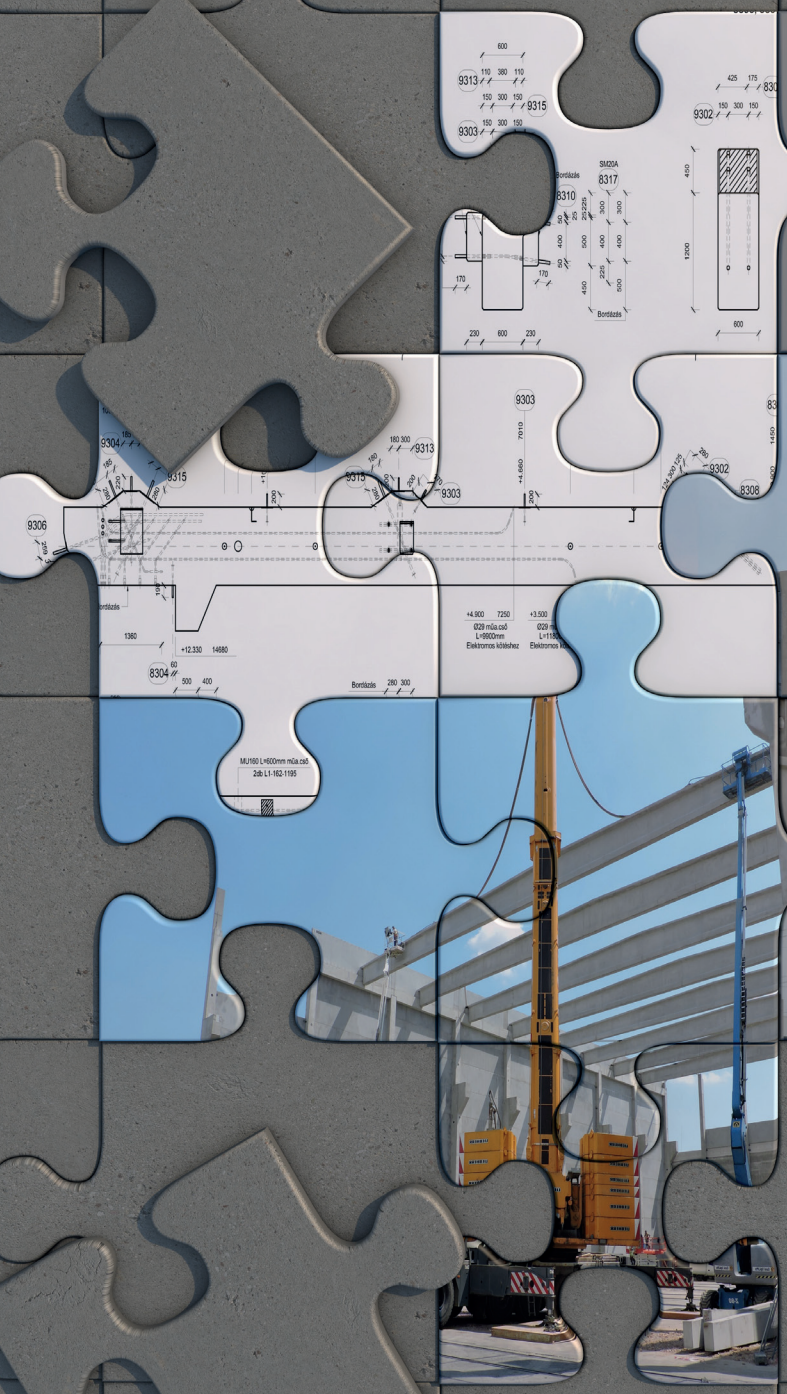





**www.ferrobeton.hu**

A-HÍD

CREATE THE FUTURE

A-Híd Zrt. I 1138 Budapest, Karikás Frigyes u. 20. I www.ahid.hu